THE MICROSTRUCTURE AND PROPERTIES OF

NIOBIUM-DOPED DIAMOND-LIKE CARBON THIN FILMS

A Thesis Submitted to the
College of Graduate and Postdoctoral Studies
In Partial Fulfillment of the Requirements
For the Degree of Master of Science
In the Department of Mechanical Engineering
University of Saskatchewan
Saskatoon
Canada

By

ADEDAYO SHERIFF ADENIYI

PERMISSION TO USE

In presenting this thesis in partial fulfillment of the requirements for a Postgraduate degree from the University of Saskatchewan, I agree that the Libraries of this University may make it freely available for inspection. I further agree that permission for copying of this thesis in any manner, in whole or in part, for scholarly purposes may be granted by the professor who supervised my thesis work or, in their absence, by the College of Graduate and Postdoctoral Studies (CGPS), Head of the Department or the Dean of the College in which my thesis work was done. It is understood that any copying or publication or use of this thesis or parts thereof for financial gain shall not be allowed without my written permission. It is also understood that due recognition shall be given to me and to the University of Saskatchewan in any scholarly use which may be made of any material in my thesis.

Requests for permission to copy or to make other uses of materials in this thesis in whole or part should be addressed to:

Head of the Department of Mechanical Engineering

57 Campus Drive,

University of Saskatchewan

Saskatoon, Saskatchewan S7N 5A9 Canada

OR

Dean

College of Graduate and Postdoctoral Studies

University of Saskatchewan

116 Thorvaldson Building, 110 Science Place

Saskatoon, Saskatchewan S7N 5C9

ABSTRACT

Doping diamond-like carbon (DLC) thin films with metals is an excellent way to reduce stresses in DLC films and improve their adhesion to artificial hip joint biomaterials. This improvement would translate to improving the implants' overall performance and ultimately extending their service life. However, limited investigation has been reported on Nb-doped DLC films in the literature. This research attempts to fill the research gap to understand the effect of Nb doping on the structure and properties of these films.

Nb-doped DLC films were deposited on silicon (100) and biomedical-grade CoCrMo alloy substrates by radio-frequency magnetron sputter technique with different Nb contents. The structure of the deposited films was characterized using X-ray diffraction (XRD), Raman spectroscopy, and X-ray photoelectron spectroscopy (XPS). Rockwell C indentation, nanoindentation, optical profilometry, and pin-on-disc wear testing were used to obtain the mechanical and tribological properties of the films. The corrosion behavior of the films in NaCl were also investigated using a potentiostat. It was found that the doped films show a nanocomposite structure with DLC as matrix and nanocrystalline Nb or Nb-C as the dispersed phase. As Nb incorporation decreases sp^3 bonded carbon bonds in the thin films, the hardness of the doped DLC films is slightly reduced. Despite this slight reduction in hardness, Nb doping drastically reduces the compressive stress in the DLC films and thus enhances the films' adhesion to the substrate. Additionally, Nb-doped DLC films reduced the wear of polymer counterparts compared to the CoCrMo alloy without coating or DLC film without doping. Likewise, the corrosion resistance of the coated substrates, especially those with Nb-doped DLC, was at least 82 % higher than the uncoated ones.

ACKNOWLEDGMENT

TABLE OF CONTENTS

LIST OF TABLES

LIST OF FIGURES

ABBREVIATIONS

ASTM	American Society for Testing and Materials
a.u.	arbitrary unit
CFUBMS	closed field unbalanced magnetron sputtering
Co-Cr	cobalt-chromium
COF	coefficient of friction
dc	direct current
DLC	diamond-like carbon
FWHM	full width half maximum
Nb	niobium
Ni-Cr	nickel-chromium
PECVD	plasma enhance chemical vapor deposition
PIII&D	plasma immersion ion implantation and deposition
PVD	physical vapor deposition
rf	radio frequency
RSF	Relative Sensitivity Factor
SBF	simulated body fluid
SCF	strong carbide former
SS	stainless steel
THA	total hip joint arthroplasty
Ti	titanium
THA	Total hip joint arthroplasty
UHMWPE	ultrahigh molecular weight polyethylene
WCF	weak carbide former
XRD	x-ray diffraction
XPS	x-ray photoelectron spectroscopy

CHAPTER 1

INTRODUCTION

1.1 **Research motivation**

As we age, so do the parts of our body. For example, the bones and joints around the knee and hip of humans are susceptible to osteoarthritis – a degenerative joint disease usually attributed to old age. Additionally, excess body fat and injury are other growing reasons for this disease. The typical way of treating this disease is by replacing the damaged joints with a prosthesis in a procedure known as total hip replacement or total hip arthroplasty. Humans' complex in vivo nature requires that these joint prostheses be made of biomaterials with excellent biocompatibility, mechanical, wear, and corrosion-resistant properties. Also, it is crucial these biomaterials last long without adverse inflammatory responses. Stainless steels, cobalt-chromium (Co-Cr), nickel-chromium (Ni-Cr), and titanium (Ti) based alloys are the commonly used biomaterials for the manufacture of the metallic components of hip and knee joint prosthesis. Polymeric materials such as ultra-high molecular weight polyethylene (UHMWPE) are also used in other parts of this prosthesis.

When hip and knee prosthesis made from these biomaterials perform their desired functions in vivo, they degrade over time due to load-bearing activities in a complex articulating system consisting of corrosive tissues and fluids. The use of stainless steel in biomedical applications has been limited over time due to its high toxicity, poor corrosion, fatigue failure, and wear resistance [1]. Cobalt is cytotoxic and is released as ions during the corrosion process in vivo. Additionally, excessive wear debris leading to adverse tissue response is experienced when UHMWPE is used in load-bearing applications [2]. Most of these degradations occur at the surface of these materials and may, in turn, lead to loosening of the implants and ultimate failure. Therefore, efforts are devoted to enhancing these implants' surfaces to extend their lifespan without considerable loss of their bulk properties. One such way is to deposit diamond-like carbon (DLC) thin films or coatings onto these implants' surfaces.

Diamond-like carbon (DLC) thin films are biocompatible with excellent physical and chemical properties such as high hardness, chemical inertness, good wear, and corrosion resistance and thus are a promising coating material to modify the implant surface. These coatings exhibit these exceptional properties partly due to the presence of a good amount of sp^3 carbon bonding. Nevertheless, previous research attempts showed that the poor adhesion of DLC to the implant substrates due to its high residual stress presented a big issue. One way to address this issue is to dope DLC with strong carbide forming transition metals such as Ti, Cr, W or use them as interlayers between the implant (substrate) and the coating.

Niobium, Nb, is an example of a transition metal with good carbon forming abilities [3–9]. Furthermore, it has been shown to possess excellent biocompatibility [10,11] and excellent corrosion resistance over a wide range of pH [12,13]. However, unlike popularly used metal dopants (such as Ti, Cr, Ag), research on niobium-doped DLC (Nb-DLC) thin films has been minimal. Most of the Nb-doped DLC films reported in the literature have been prepared on Fe and Ti-based substrates [6,7,14–21], and none has been deposited unto CoCrMo substrates. Furthermore, most of the published data on Nb-DLC films consisted of hydrogenated DLC [6,7,14–18] with little information about Nb-doped non-hydrogenated DLC films. Lastly, Nb-DLC's wear behavior against ceramic counterpart has been reported [7,8,17], but report on Nb-DLC sliding against polymer counterparts .

1.2 Research objectives

Of all the alloys listed in the first paragraph, the American Society for Testing and Materials (ASTM) F-75 (Co-Cr-Mo) alloy is often used in knee and hip prosthesis as femoral and acetabular components. Therefore, the primary goal of this research is to enhance the wear and corrosion resistance of this alloy by applying adherent Nb-DLC thin films onto its surface. To achieve the goal, this thesis work has three tasks as follows:

- Synthesize Nb-DLC coatings with different Nb concentrations and evaluate the effect of niobium concentration on the structure of the Nb-DLC films.
- Understand the effect of Nb concentration on the mechanical and corrosive properties of the coatings, including hardness, residual stress, adhesion, tribological behavior, and corrosion resistance.

- Enhance the adhesion of DLC films on CoCrMo alloy discs by doping DLC with Nb and applying Nb interlayer.

1.3 Contribution to existing knowledge

- Nb-doped non-hydrogenated DLC films with excellent adhesion on CoCrMo alloys were synthesized.
- The doped thin films can significantly reduce the wear rate of UHMWPE.
- The doped thin films show better corrosion resistance.

1.4 Thesis outline

Chapter 1 begins with a concise introduction, focusing on the motivation and objectives of this research.

In chapter 2, a detailed but relevant literature review is presented.

In chapter 3, the experimental methods, including materials preparation, deposition techniques, and the techniques and tools for structural and property characterization were discussed.

The results and discussion were presented in chapter 4. In the first section of this chapter, the effect of increasing Nb concentration on the film structure is discussed. In subsequent sections, the effect of Nb on the mechanical properties, tribological and corrosion behavior of the films is expounded.

Finally, concluding remarks and recommendations are presented in chapter 5.

CHAPTER 2

LITERATURE REVIEW

Materials scientists and engineers are striving to continually improve the properties of the existing materials and to develop tools and techniques for effectively characterizing them. This chapter will present an overview of the different materials used for artificial joint applications, the main issues relating to the applications, and how metal-doped diamond-like carbon films are being used to address some of these issues. Lastly, the standard techniques used to prepare these films will be elucidated.

2.1 Materials for hip arthroplasty

Total hip joint arthroplasty (THA) is a conventional method used to treat diseased or damaged hip joints. This process, which has been nicknamed the surgery of the century, involves replacing these joints with artificial implants. An example of a hip implant is shown in Figure 2.1. In many of these implants, the bearing system is usually made of materials combined in different configurations, each having its pros and cons. The most used combinations typically have at least a metal component in order to have sufficient mechanical strength and toughness to withstand loads and impact [22]. The metals or alloys conventionally used in the design of implants are stainless steels, Ti and its alloys, and CoCrMo [23,24].
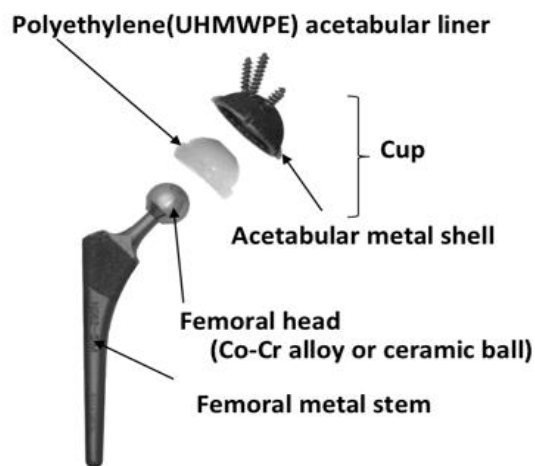
Figure 2.1. A schematic diagram of the hip implant [25]

2.1.1 Stainless steel alloys

In the 1960s, the first-ever successful THR procedure was performed by replacing a damaged joint with an implant having a femoral head made from AISI 316L austenitic stainless steel (SS) [26,27]. Prior to this, stainless steels have been used for other types of internal fixations. Its extensive usage is due to an acceptable level of mechanical properties, corrosion resistance, biocompatibility, and cost-effectiveness. However, owing to the release of Ni, stainless steel is prone to pitting, crevice, and stress corrosion and has also been reported to be responsible for allergic reactions in patients. [28,29]. In a study to understand the release of ions and constituents of 316L stainless steel, it was found that after immersing the steel in a simulated body fluid (SBF), Ni, Fe, and Cr were released into the fluid [30].

Over the years, several efforts have been directed towards enhancing the properties and performance of stainless steels by modifying the amount of constituent elements. However, owing to the dissolved oxygen and chloride in body fluids, corrosion of implants is still very likely. Coating and surface modification techniques including but not limited to anodization, passivation, and glow-discharge nitrogen-implantation has been used to improve the corrosion resistance, wear resistance, and fatigue strength of 316L stainless steel [31]. Jin et al. prepared Ti-Cu films on 316L stainless steel substrates using a closed field unbalanced magnetron sputtering (CFUBMS). The films showed improved corrosion and wear resistance in a simulated body fluid (SBF) [32]. Antibacterial activity was also reported to be significantly improved. Although initial prosthetic designs used stainless steel, it has been discontinued over the years due to its apparent issues, and other metallic alloys have been used.

2.1.2 Titanium and its alloys

Ti and its alloys are extensively used in the biomedical field owing to their lightweight, excellent mechanical properties, and corrosion resistance [31]. Most important is that their biocompatibility with bones is outstanding [27]. Unalloyed Ti metal also known as cpTi, has long been used with a high success rate in dentistry. This metal has been found increased use in several other biomedical applications following its successful use for bone plates and screws in the mid-60s. As such, it has been standardized for surgical implant application in ASTM F67 [33]. The good properties of Ti

alloys are partly attributed to its formation of a protective passive oxide film. Shukla et al. [34] showed from their investigation that the passive oxide film formed on Ti provided more corrosion resistance compared to Ti–6Al–4V when tested in Hank's solution.

Although Ti has been proven to have excellent props, there are a few reservations. Firstly, it can present some esthetic issues with soft tissues [28]. More recently, attention has been drawn to the likelihood of toxicity due to the release of Ti ions and particles into surrounding tissues due to wear and corrosion, leading to yellow nail syndrome and hypersensitivity reactions [35]. Due to these issues, Ti is usually alloyed with other materials such as Al, V, Fe, Sn, Zr, Ta, Nb, etc., to improve its properties by stabilizing phases present in Ti.

In applications involving musculoskeletal systems, Ti_6Al_4V is the most used Ti alloy. This is due to their combination of good mechanical properties, appreciable corrosion resistance, and good biocompatibility [26,31]. However, owing to the insufficient ductility and low protection exerted by Ti surface oxides, which results in poor wear properties, conventional Ti alloys are not used to manufacture femoral components of implants. [27,29]. Also, the release of alloying elements, which may be toxic, leading to inflammatory response, is of concern. To avoid these limitations, materials scientists have developed new Ti alloys having better potential for orthopedic applications. Some of these alloys are biomedical applications are TiAlNb, TiAlNbTa, TiNbTaZr, TiSnNb, TiNiTa [31]. Although many of these alloys involve alloying with Nb and or Ta, they still contained elements that could be toxic and released to the in vivo environment. Therefore, the requirement of an overlay that is biocompatible and possesses similar mechanical properties as the alloy is much needed.

2.1.3 Cobalt–chromium alloys

CoCr alloys have been extensively used in several biomedical applications such as dentistry, oral and maxillofacial surgery, and orthopedics for knee and hip implants. This is due to their acceptable level of biocompatibility. Before their use as biomaterials for medical devices, they have been a major alloy in aircraft engine design due to their outstanding mechanical properties, wear, and corrosion-resistant properties. Following the successful use of these alloys in the aircraft industry and their lower wear rates than stainless steels and titanium alloys [29,31], they are being

used to manufacture knee and hip implants' femoral components, which are subjected to loading and wear. Ti alloys, however, have higher biocompatibility.

The major elemental components responsible for the excellent properties of these alloys are; Co, which provides the continuous phase; Cr, responsible for corrosion resistance and Mo; providing strength and bulk corrosion resistance [28]. In other alloy types, an appreciable amount of nickel, Ni can be found. The CoCr alloy consisting of mainly Co, Cr, and Mo is called cast-alloy type. That, in which Ni is present, is the wrought-alloy type. The former, having a composition, $CoCr_{29}Mo_5$ (ASTM F75, ISO 5832-4), is mostly used in orthopedics for manufacturing femoral heads, while the latter, having the composition, $CoNi_{35}Cr_{20}Mo_{10}$ (ASTM F562), is used in making the stems of orthopedic prosthesis due to their high strength requirements [26].

Huang et al. [2] studied the friction and wear behavior of cast and wrought Co-Cr implant alloy in a dry sliding wear test by sliding the alloy against ultrahigh molecular weight polyethylene (UHMWPE). The steady-state coefficient of friction for cast and wrought Co-Cr alloys were 0.220 and 0.245 respectively, while the specific wear rates were $1 \cdot 80 \times 10^{-7}$ and $2 \cdot 78 \times 10^{-7}$ mm^3 N^{-1} m^{-1} for cast and wrought alloys, respectively. It is seen that the cast Co-Cr alloy has slightly better wear properties, which is why it is mainly used for the femoral part of hip and knee implants. Furthermore, the wear properties of wrought Co-Cr alloy is further reduced when sliding against itself or other material types. Also, the presence of Ni, which can be present to a maximum amount of 37 at. % raises toxic and allergenic concerns because it is usually released in vivo. Likewise, even at smaller amounts, the release of Co can result in the death of some cells. Although Cr is non-toxic, in vitro experiments have shown that its release due to aseptic loosening is likely, and has the potential of causing cancer [31].

2.1.4 Limitation of current metallic biomaterials

Over the years, many different metals, primitive or advanced, have been used as implants. However, no material is a hundred percent perfect. In recent orthopedic procedures, femoral heads made from SSs, Ti alloys, and Co-Cr alloys are primarily used because each material combines good mechanical properties (see Table 2.1), as well as acceptable biocompatibility. However, due to surface interaction between these implanted biomaterials and the biological environment, they

7

tend to release metallic ions in this environment resulting in toxic effects such as cancer, inflammation, hypertension, osteolysis, etc. Furthermore, implants may be exposed to load-bearing activities and an environment containing corrosive bodily fluids and tissues, which causes them to wear and corrode, often necessitating revision surgeries which are more expensive than initial replacement surgeries. Also, regarding mechanical properties, the modulus of elasticity of these alloys is far greater than that of bones, leading to stress shielding. Another mechanical property-related problem is that these metallic biomaterials have a high coefficient of friction and low surface hardness. Lastly, in metal on polyethylene implant configuration, these metals cause excessive wear of polymeric materials. Modifying the surfaces of these implant alloy materials is one the simple but effective methods used by materials scientists to address these issues. One of such methods is the coat the surfaces of these alloys with diamond-like carbon films.

Table 2.1. Mechanical properties of the bone and metallic implant materials [29,36–38]

Implant material	Elastic modulus (GPa)	Yield strength (MPa)	Tensile strength (MPa)	Elongation to failure (%)	Fatigue resistance at 10^7 cycles (MPa)	Fracture toughness MPa.m$^{1/2}$	Hardness (GPa)
316L SS	210	170	485	50 (20)^c	54	112 – 278	1.7 – 2.2
Ti and Ti alloys	110 – 120	485 – 830	760 – 1000	15 – 25	300 – 700	84 – 107	3.4 – 3.7
CoCrMo alloy	200 – 300	450-800	735	1 – 10	200 – 950	100	7.99
Bone (compact)	15 – 20	30 – 70	70 – 150	0 – 8	< 40	2-12	–
UHMWPE	0.6 – 1.8	–	23 – 40	200 – 400	36	–	–

2.2 Diamond-like carbon (DLC) coatings

The joint implant bearing combinations having at least one metal, such as metal-on-metal (MOM) and metal-on-polymer (MOP), have been extensively used in orthopedics. However, metal ion release and wear debris from the metals lead to complicated medical issues. Likewise, a large amount of wear debris is generated in bearings containing polymeric materials, which is also potential for adverse medical reactions. Diamond-like carbon (DLC) films are usually deposited

8

on both metallic and polymeric surfaces to mitigate these challenges. There are many publications to show the extent of research in this area (Figure 2.2). In this section, a review of the benefits and limitations of DLC is presented. Also, previous studies where DLC films have been doped with metals to improve their properties, are discussed. Also, the commonly used surface deposition techniques will be discussed.
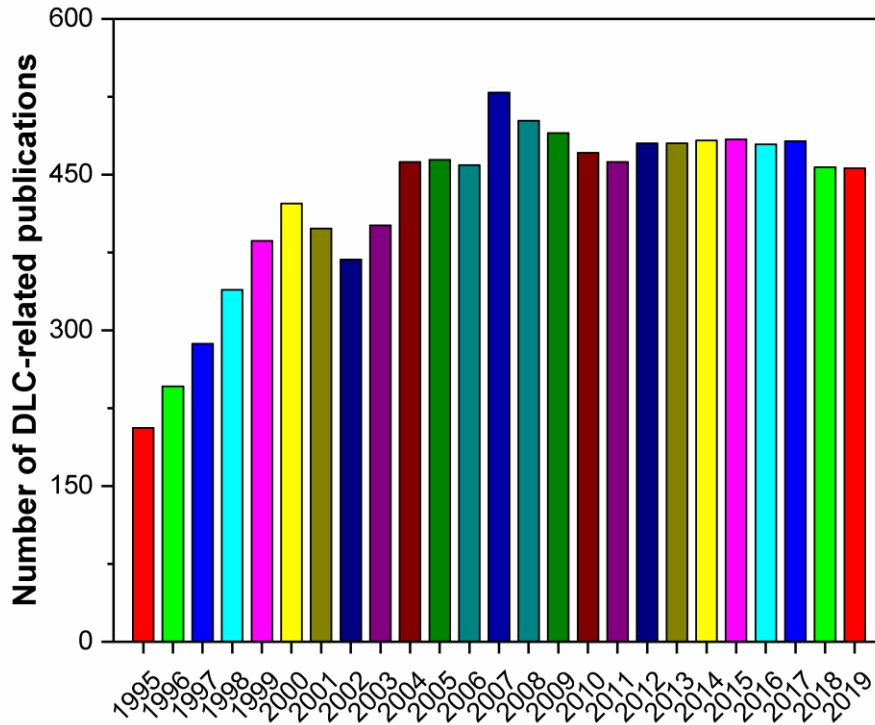
Figure 2.2. The number of publications on diamond-like carbon between 1996 and 2019 (data obtained from the web of science excluding 2020)

The term diamond-like carbon has been popularly described using the ternary phase diagram shown in Figure 2.3. DLCs are a class of amorphous carbon coatings consisting of sp^2 and sp^3 bonded carbon in varying proportions and different amounts of hydrogen. Depending on the relative amount of each constituent, DLC films can have different structures and properties. DLC films generally are amorphous surface coatings used in several applications due to their anti-sticking ability, biocompatibility, chemical inertness, low friction coefficient, high hardness, and good wear resistance. Table 2.2 shows the structure and properties of different DLCs. When the

9

amount of sp^3 is considerable compared to sp^2 and H, the DLC film exhibits properties similar to that of diamond. Hydrogen-free tetrahedral amorphous carbon (ta-C) and hydrogenated tetrahedral amorphous carbon films (ta-C:H) are a class of DLC films characterized with the highest fraction of sp^3 hybridized carbon atoms. Hydrogenated amorphous carbon films (a-C:H) on the other hand, have a higher amount of H and sp^2 but lesser sp^3 bonded carbon. As a result, they have been reported to possess a lower friction coefficient in dry tribological tests due to the softer graphitic phase. However, films having more sp^3-C and low H content have higher wear resistance [39].
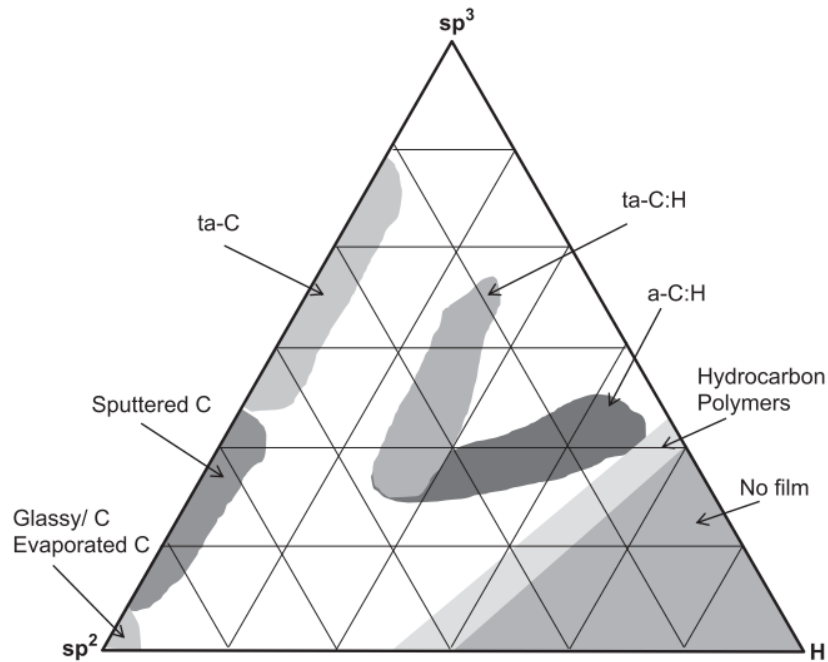
Figure 2.3. Ternary diagram for DLC formation with respect to sp^2, sp^3 and hydrogen content [40]

Table 2.2. Structure and properties of diamond and diamond-like carbon films[40]

		Coating Materials				
		Diamond	ta-C	ta-C:H	a-C:H	
					Hard	Soft
Processing temperature		> 700 °C	room			
Structure		Cubic - crystalline	Amorphous	Amorphous	Amorphous	
Properties	sp^3-C (%)	100	80 – 88	70	40	60
	H (%)	0	0	30	30 – 40	40 – 50
	Hardness (GPa)	100	80	50	10 – 20	< 10
	Density	3.52	3.1	2.4	1.6 – 2.2	1.2 – 1.6
	Friction	0.01 – 0.5				
	Band gap (eV)	55	2.5	2.0 – 2.5	1.1 – 1.7	1.7 – 4

Among the several thin film deposition techniques, the several variants of physical vapor deposition (PVD) and plasma-enhanced chemical vapor deposition (PECVD) are the mostly used. Each of these has different peculiarities that affect the structure and property of the DLC film. With the PVD magnetron sputtering technique, the atoms of the target (solid) materials are vaporized, transported through vacuum, and condensed onto substrates materials. The PVD process can be operated in both rf (radio frequency) and dc (direct current) and has been used to prepare non-hydrogenated DLC coatings with high sp^3. A graphite is used as the target material for these films to ensure H is not present. Hydrocarbon sources such as C_2H_2 (acetylene) and CH_4 (methane) are used to synthesize films hydrogenated DLC films. This is mainly done using the PECVD technique. In both methods, the DLC films, because of the high energy process of deposition, have embedded in them compressive intrinsic stresses, which cause poor adhesion and ultimately limit industrial-wide application. The stress may be as high as 10 GPa. Other problems with DLC films are low toughness [8], poor thermal stability [41] (for films deposited at high temperature), and poor wear resistance at high temperature [42] (this is not necessarily important for films deposited on hip and knee implants because they do not operate at high temperatures). Most of these limitations have been solved by doping/alloying the DLC structure with metallic and non-metallic elements.

2.3 Metal-doped diamond-like carbon (Me-DLC)

To overcome the challenges of DLC films, Dimigen and Hübsch in 1992 prepared the first metal-doped diamond-like carbon films. In their work, metal targets such as Ta, W, Ru, Fe, and Si were sputtered in a vacuum chamber consisting of argon and acetylene gas to produce 0.9 µm thick a-C:H:Me films [43]. Their films were reported to be with improved tribological properties [43]. Similarly, the first metal-doped non-hydrogenated DLC (a-C:Me) films were prepared by Eckel et al. [44]. An increase in Zr and Ti concentration was found to cause an increase in hardness and critical load required for failure. In later years and up till now, several other metals such as Ag, Al, Au, Cr, Cu, Ni, Nb, Ti, etc. have been used to dope DLC films, all with the aim of reducing internal stress and improving adhesion, biocompatibility, friction, and wear properties. Doping DLC with metals can be done through different routes such as:

  i.   Single metal doping [45]
  ii. Doping a metal-doped DLC with a second metal [42]
  iii. Co-doping of two metal simultaneously [46]

Depending on the nature and amount of metal content in the DLC, they may either bond with the carbon (to form metal carbides) or exist as metal nanoparticles [47]. With respect to the nature, metals are classified as either weak carbide formers (WCFs) or strong carbide formers (SCFs). Aside from their carbon forming or bonding abilities, the major difference between both metal types is that DLC films' hardness and tribological properties can be improved when doped with a small amount of SCFs. For instance, when Ti-doped DLC with 0 wt. % to 18.29 wt. % of Ti, the highest hardness and lowest wear rate was observed with 1.82 wt.% Ti [48]. A similar result was reported by Ding et al. [8], where the highest hardness and lowest wear rate was observed with 1.28 at.% Nb incorporated into a:C films. In most cases, the small amount of doped metals either dissolve into or exist as nanocrystallites of metal carbides in the DLC matrix [49,50].

Irrespective of the metal-type, a reduction in hardness of DLC films is usually experienced when doping with metals. For SCFs, higher amount of metals results in the formation of larger metal carbide (Me-C) particulates, which ultimately results in deterioration of mechanical and tribological properties. In the Cr-DLC films prepared by Wei and Aiying, it was observed that at higher Cr amounts, the tribological properties of DLC deteriorated [51]. Others have reported a

12

similar trend for Ti-DLC, such as Jinfeng et al. [52] and Yefei et al. [48]. Contrary to these results, improvement of mechanical properties at a higher concentration of Ti was reported in the work of Mengqi et al. [53] when Ti-DLC was prepared by dual magnetron sputtering. Concerning WCFs, metals such as Al and Ag, caused a drastic reduction in hardness and tribological properties, because these metals, when introduced into the carbon matrix, form the soft and ductile clusters, rather than bonding with carbon atoms [46].

Coatings with internal compressive stresses greater than 1 GPa are prone to delamination leading to catastrophic failure [54]. This stress is often calculated using Stoney's equation (Eq. 1.1). When DLC films are doped with metals: irrespective of their nature or amount, the internal stress is usually reduced, and adhesion is improved, making them suitable for tribological applications. The adhesion strength can be measured qualitatively by comparing the imprints from a Rockwell C indentation to the principle of Verband Deutscher Ingenieure, VDI 3198 indentation test (Figure 2.4) [55]. Likewise, scratch testing in which a diamond indenter is dragged across a surface with either constant or progressive loading is used to understand the adhesion behavior of films. The high internal stresses in DLC are usually attributed to the higher sp^3 bonded carbon atoms. The introduction of metals into the DLC network results in the relaxation of distorted length and bonds, leading to reduced stress [8,48].

$$\sigma = \left(\frac{1}{R_2} - \frac{1}{R_1}\right) \frac{E_s}{6(1-\nu_s)} \left(\frac{t_s^2}{t_f}\right) \ldots\ldots\ldots\ldots\ldots \text{Eq. 1.1}$$

Where:
- o R$_1$ and R$_2$ are the radius of curvature of the substrate before and after deposition.
- o E_s and ν_s are the substrate's modulus of elasticity and the Poisson's ratio.
- o t_s and t_f are the substrate and coating thicknesses.
- o σ is the internal compressive stress.
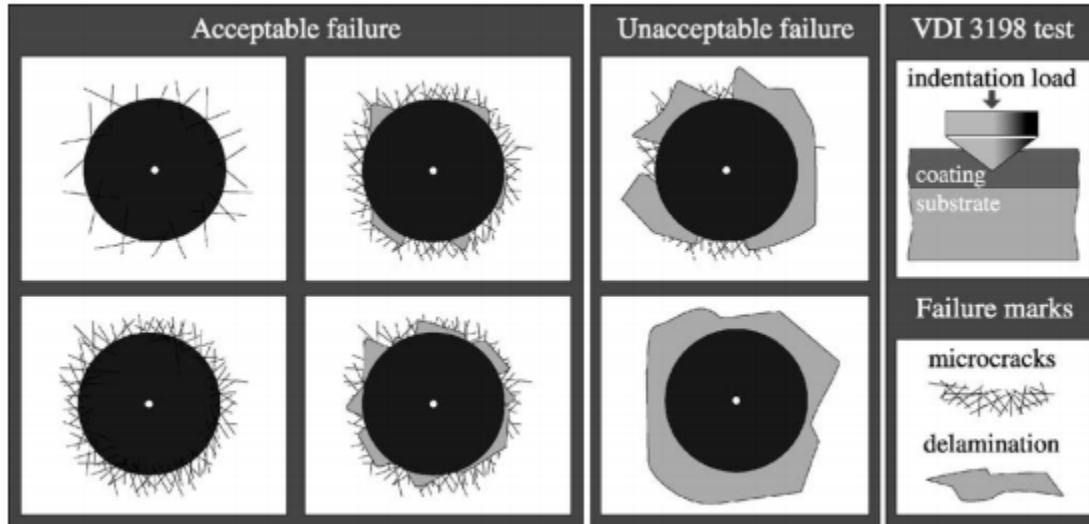
Figure 2.4. The principle of VDI 3198 indentation test [55]

When a femoral head articulates against the UHMWPE acetabular component in orthopedic implants, the wear debris from the polymer often leads to unfavorable health consequences. Generally, among all the common metallic biomaterials such as CoCrMo stainless steels, and Ti alloys, CoCrMo causes the slightest wear to UHMWPE. In a bid to further reduce the wear of the polymer cups, Afatato et al. [56] and Vesa et al. [57], deposited DLC films unto commercial CoCrMo femoral heads and found from a wear-simulator test that the coated films slightly reduced the wear of UHMWPE cups.

2.4 Techniques used deposit Me-DLC films

Me-DLC thin films are usually deposited by physical vapor deposition (PVD) or chemical vapor deposition (CVD). Whereas undoped DLC film may be produced by CVD alone (as in the case of hydrogenated DLC), metal-doped DLC films are usually deposited by PVD or by combining both the PVD and CVD processes.

CVD is a film deposition process in which gaseous phase precursors react chemically on or near a substrate surface to ensure high-quality films with excellent conformality [58]. Pyrolysis, reduction, oxidation, nitridation, carbidization, and chemical transport reaction are some chemical reaction types used to prepare the films. Hydrogenated DLC films are usually deposited from gases

such as methane and acetylene through CVD. However, the CVD technique cannot be used to deposit metal-doped non-hydrogenated DLC films due to the need for a pure carbon source.

The PVD process refers to a variety of vacuum deposition techniques in which the film to be deposited is condensed from a vaporized solid material. Depending on the methodology used in vaporizing the target material, PVD can be classified into vacuum evaporation, ion plating, and sputtering. Sputtering is the most widely used PVD technique, and its principle is summarized in figure 2.5. Compared with other processes, sputtering has a number of advantages, such as the possibility of sputtering high melting materials, deposition of high-quality films at low temperature with a composition similar to the target material, the deposition of homogenous films, the ability to clean samples prior to deposition, and improving properties of by energetic ions [58]. Several Me-DLC films have been prepared using the sputtering technique.
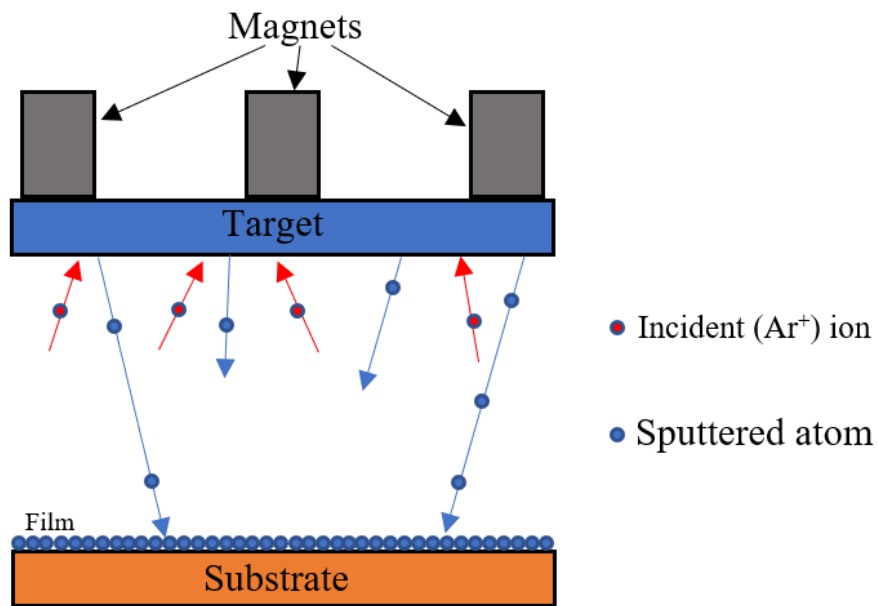
Figure 2.5. The sputtering principle

CHAPTER 3

MATERIALS AND METHODOLOGY

In this research, a magnetron sputtering system (Model: SPT320 – PLASMIONIQUE) was used to prepare the DLC and Nb-doped DLC thin films. The niobium and graphite targets were placed in magnetrons, each powered respectively by a radiofrequency and a direct current power supply. All depositions were plasma-assisted and conducted with a negative voltage bias. The concentration of Nb in the Nb-DLC films was varied by changing the Nb target power. Subsequently, the effect on the films' structure was evaluated using a variety of techniques such as x-ray photoelectron spectroscopy (XPS), Raman spectroscopy and x-ray diffraction (XRD). Also, optical profilometry, scanning electron microscopy (SEM), Rockwell C indentation, nanoindentation, tribology and corrosion testing were used to understand the properties. An overview of the materials, equipment and characterization used will be described in this section.

3.1 Materials

In this research, Silicon (Si) wafers and CoCrMo alloys were the substrate materials upon which the thin films were deposited. The n-type Si wafers have an orientation <100>, the thickness of 381±25 µm, and were manufactured by Wafer Pro Inc. The Si substrates were used for residual stress calculation. The CoCrMo rods, whose composition was similar to standard ASTM F1537 biomedical implants [59], were manufactured by M. Vincent & Associates Inc. The composition of the CoCrMo alloy is shown in Table 3.1. These rods were cut into cylindrical disks of a diameter of 25.4 mm, and a thickness of 3.15 mm. The sputtered targets: niobium and graphite (99.9 % purity), were produced by Plasmionique Inc.

Table 3.1. Chemical composition of the CoCrMo [59]

Element	Composition (%) (mass/mass)
C	0.14
Cr	30.00
Mo	7.00
Ni	1.00
Fe	0.75
Si	1.00
Mn	1.00
Ni	0.25
Co	Balance

3.2 Thin film deposition

3.2.1 Sample preparation

Using SiC abrasive and diamond suspension, the alloy discs were ground and polished to achieve a mirror-like surface finish. To achieve this finish, the discs ground in a stepwise manner using #80, #180, #320, and #800 SiC grits followed with 9, 3 and 1 µm diamond suspension. Also, Si wafers were cut into a rectangular geometry (in a ratio of 1:10) to measure radii of curvatures. To remove contaminations, the substrate materials were ultrasonically cleaned in acetone for 30 minutes.

3.2.2 Magnetron sputtering

The DC/RF magnetron system in which graphite and niobium targets were installed was used to prepare the DLC and Nb-DLC thin films. The system was selected to enhance the sputter yield of graphite target [40]. Other advantages are the possibility of depositing high purity films with high adhesion and ease of automation [60]. A schematic of this system is shown in Figure 3.1. It is equipped with a vacuum chamber, a pumping system (not shown in the schematic) whose primary function is to keep the chamber in vacuum (up to 10^{-8} Torr). There are three magnetrons in the vacuum chamber, each of which can be connected to either a direct current or radio frequency power source. The targets to be deposited are usually placed in the magnetrons (or cathodes) whose

primary function is to keep electrons in the plasma close to the surface of the target material, leading to enhanced ionization, constrained plasma, and increased sputter deposition rate at a low gas pressure. This plasma is usually created by ionizing an inert gas (Argon). Lastly, one remote inductively coupled Plasma (ICP) source, and a substrate holder connected to a heater module are in the chamber.
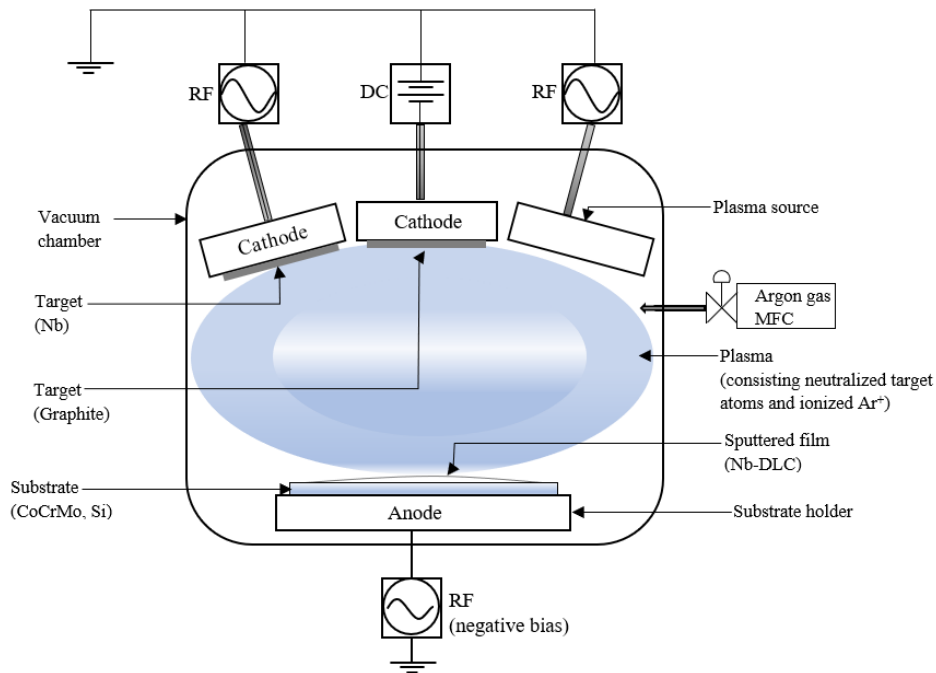
Figure 3.1. Schematic of the dc/rf plasma-assisted physical vapor deposition system

After cleaning by ultrasonication, the niobium doped thin films were deposited following the sequence of the following steps:

- Firstly, Ar ion cleaning of the targets and substrates was done at a substrate bias of 163 V and Ar flow of 30 sccm.
- This was followed by the deposition of a Nb interlayer with 200 W target power and substrate bias of 73 and 163 V for 20 minutes. This function of the interlayer is to enhance the adhesion of DLC films to the substrate.
- Lastly the Nb-DLC layer was deposited by varying the rf power to the Nb target from 0 to 50 W. The dc power to the graphite target was constant at 300 W. The substrate bias,

Table 3.2. Deposition conditions of the DLC and Nb-DLC films

	Nb-DLC	DLC	Nb interlayer
Nb target (rf) power (W)	20, 25, 30, 40, 50	0	200
Graphite target (dc) power (W)	300		-
Substrate bias (V)		163	
Plasma power (W)	200		-
Argon flow (sccm)		30	
Substrate temperature (^{o}C)		< 80	
Substrate rotation (rpm)		3	
Deposition time (minutes)	180		20
Working pressure (Pa)		1.33	
Base pressure ($*10^{-5}$) (Pa)		~1.33	

3.3 Thin film characterization

3.3.1 X-ray diffraction (XRD)

Conventional $\theta/2\theta$ XRD methods are usually not suitable for thin films because the diffraction signals from the films are too weak to be observed. On the contrary, a 2θ scan with a fixed grazing angle of incidence, popularly known as grazing incidence XRD (GIXRD), is ideal. The angle between the incident x-ray and the surface of the sample is fixed and usually less than 5°. A rule of thumb is that this angle should be slightly above the critical angle for total reflection of the film material. A schematic of this process is shown in Figure 3.2.

In this study, all films were characterized by GIXRD to identify the structural changes and the evolution of phases. A Rigaku Ultima IV X-ray diffractometer in grazing incidence configuration equipped with Cu-Kα radiation (wavelength = 0.15406 nm) was used. The incident angle, x-ray

voltage and current were 2°, 40 KV and 44 mA respectively. X'Pert HighScore (version 2.1.1) was the software package used to analyze the XRD patterns.
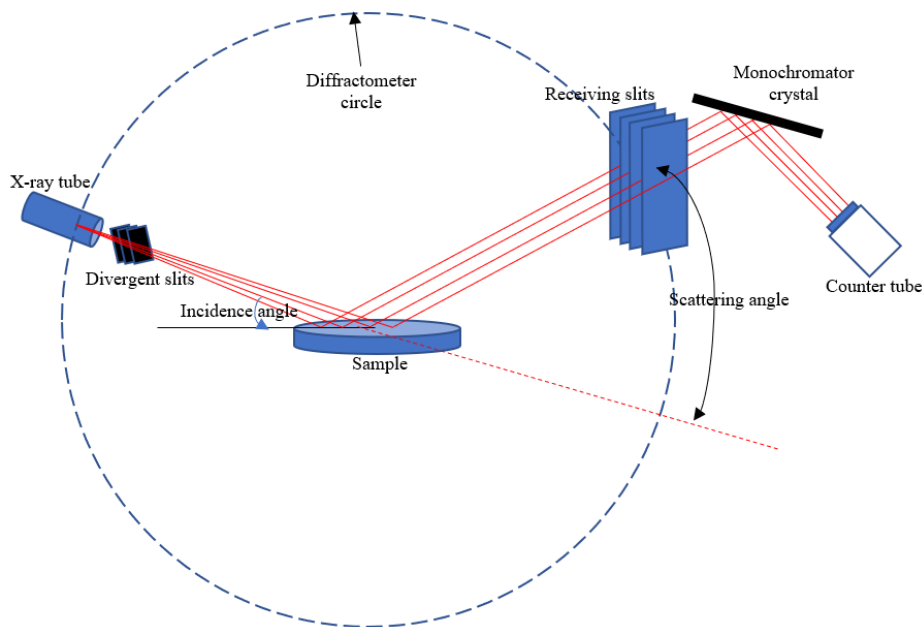
Figure 3.2. Schematic of the measuring arrangement for thin films by GIXRD

3.3.2 Raman spectroscopy

Raman spectroscopy is an analytical technique that utilizes the interaction of light and the molecules of a material to gain insight into chemistry of that material. In this technique, a high intensity light source (usually a laser) interacts with the molecules of a material, resulting in scattered light having wavelengths similar (elastic) and different (inelastic) to that of the incident laser. The inelastically scattered light (orange line), also known as Raman shift, provides useful information about the material's bonding states. A schematic of this process is shown in Figure 3.3.

The carbon-carbon bonding structure in the Nb-DLC films were analyzed using a Renishaw Invia Raman microscope (Renishaw, Gloucestershire, UK). The high intensity light source used was a laser beam of wavelength of 514.5 nm. Before each test, the system was calibrated internally using silicon characteristic peak at 520 cm^{-1}. The resulting Raman spectra of DLC-based samples feature mainly two peaks, showing the intensity and the Raman shifts. These peaks are known as D and

G bands. The D band (disordered/defect and not diamond) which is usually found around a Raman shift of 1300 – 1380 cm^{-1} originates from a hybridized vibrational mode associated with aromatic rings or graphene edges [61]. The G band (graphitic) with a Raman shift of 1500 – 1630 cm^{-1} is caused by stretching vibration of sp^2 lattice mode [61]. Wire 3.3, a dedicated software package for Raman spectroscopy, was used to analyze the results.
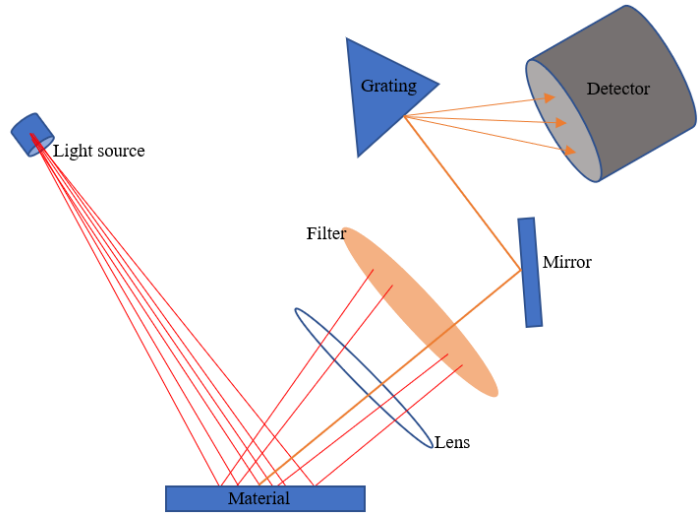
Figure 3.3. Raman spectroscopy schematic

3.3.3 Xray photoelectron spectroscopy (XPS)

XPS is a non-destructive analysis where x-rays in an ultra-high vacuum environment are made to interact with the surface of materials, leading to emitted electrons whose kinetic energy are immediately measured. The binding energy of each atom is subsequently calculated based on the relation.

$$E_b = h_v - E_k - \phi_w \ldots\ldots\ldots\ldots\ldots \text{Eq. 3.1}$$

Where:

E_b = binding energy

h_v = incident energy of the X-ray photons.

E_k = kinetic energy

ϕ_w = work function

The result of the XPS characterization is a spectrum showing a plot of photoelectron intensity against binding energy. Since each electron will have a characteristic binding energy, each peak from this spectrum can be assigned to specific element and area. Also, the area under the peaks can be quantified to obtain information on the electronic states of atoms in the surface region. XPS could also be a semi-destructive analysis when it is utilized for depth profiling. In this mode, the spectrum of the topmost layer of a film surface is recorded. This is followed by sputtering the film surface with Ar^+, after which the spectrum of the revealed layer analyzed and recorded. This cycle is continued to obtain subsurface information further.

In this thesis, Axis Supra X-ray photoelectron spectroscope by Kratos Analytica was used to obtain the films' elemental composition and chemical bonding states. This device is operated under high vacuum and is equipped with a 500 mm Rowland circle monochromated Al Kα (1486.6 eV) x-ray source to provide excellent energy resolution. It also has a depth profiling option which was used to probe the subsurface of the Nb-DLC films. Survey spectra for both the top surface and subsurface of the films were obtained within a binding energy range of -5 and -1200 eV. Also, high resolution scans for the carbon and niobium regions were performed within 277 – 300 eV and 199 – 212 eV respectively.

The x-ray diffractometer, Raman spectrometer, and x-ray photoelectron spectroscope used in this thesis were at the Saskatchewan Structural Science Centre (SSSC), the University of Saskatchewan.

3.3.4 Rockwell C Indentation

Rockwell C indentation is an easy method used to determine the adhesion of coatings and thin films qualitatively. In this test, a load of 1470 N is applied on the films through a diamond cone indenter. This results in a circular impression which is checked for cracks and delamination using either an optical microscope or an SEM. The image is compared with the VDI 3198 guideline shown in figure 2.4 to determine whether failure is acceptable or unacceptable. In this thesis, the Instron Wolpert GmbH Rockwell C hardness tester in the Department of Mechanical Engineering, University of Saskatchewan was used to examine the adhesion behavior of the Nb-DLC films.

3.3.5 Scanning electron microscopy (SEM)

The SEM uses focused high-energy electrons to raster over the surface and subsurface of solid materials to generate signals that provide information about the micrography of the surface. The SEM used in this thesis is a Jeol JSM-6010LV SEM at the Department of Mechanical Engineering, University of Saskatchewan. This equipment was used to examine the imprints after Rockwell C Indentation tests.

3.3.6 Optical profilometer

Zygo NewView 8000 optical profiler was used in this study to measure the thickness of this films. Before deposition, a temperature-resistant tape is placed over a section of the substrate to avoid film being deposited on that section and create a height difference between the coated and uncoated areas. Based on this step height, the film thickness is measured. Also, the radius of curvature of the substrate before and after deposition was measured with this equipment. Based on the obtained radii and the Stoney's equation (Eq. 1.1), the internal compressive stresses in the films were calculated. Also, after the tribological testing (explained in section 3.3.8), the wear volume of the films was obtained using the optical profilometer.

3.3.7 Nanoindentation

Nanoindentation is an important technique to measure the mechanical properties of thin films. Properties such as hardness, elastic modulus, fracture toughness, and creep may be obtained. In this thesis, a Center for Tribology (CETR) Universal mechanical tester (UMT) was used to measure the micohardness and Young's modulus of the Nb-DLC films. This was achieved by applying a load through a Berkovich indenter that penetrates the films. In this thesis a load of 3 mN was used to avoid substrate's influence. A general rule of thumb to avoid substrate's contribution is that the indentation depth should be < 10% of the film's thickness. To ensure correctness and reproducibility, more than 15 indents were performed. The unloading of the indenter completes the indentation cycle.

3.3.8 Tribology testing

In this thesis work, a pin-on-disk tribo-tester, also manufactured by CETR Inc., was used to investigate the tribological behavior of the samples. This test method involved the surfaces of two materials rubbing against each other. The other material, often called a counterpart, is a cylindrical-shaped UHMWPE pin. This pin is fixed and made to slide in a linear reciprocation motion against the thin films. This test aims to obtain the coefficient of friction of the tribo-pairs as well as the wear rates of the UHMWPE and Nb-DLC films. In these experiments, UHMWPE pins (diameter = 4.5 mm) slid against uncoated CoCrMo alloy disks, undoped DLC, and Nb-DLC in a distilled water solution at room temperature. For the entire duration (10,000 seconds), a constant load of 10 N was applied over a sliding distance of 250 m. The wear rates of the pins and films were subsequently calculated using Eq. 3.2.

$$K = \frac{V}{NL} \ldots\ldots\ldots\ldots \text{Eqn. 3.2}$$

Where:

V is the pin's volume loss, N is applied load, and L is total sliding distance.

3.3.9 Corrosion testing

To understand the corrosion behavior of the bare CoCrMo alloy, DLC, and Nb-DLC films, potentiodynamic polarization measurements were performed using a research-grade electrochemical instrument, Potentiostat/Galvanostat/ZRA (Interface 1000, Gamry Instruments) located in the Department of Mechanical Engineering, University of Saskatchewan. The electrochemical setup for this experiment (as shown in Figure 3.4) consisted of a conventional three-electrode system where the specimens to be evaluated acted as the working electrode, pure graphite rod as the counter electrode, and standard calomel electrode (SCE) as the reference electrode. The working electrodes (insert) were masked, revealing only a circular portion (1cm^2 area) in contact with the electrolyte (0.9% (w/v) NaCl). The specimens' surfaces were scanned at the sweep rate of 1 mV/s, and within −250 to +250 mV range, relative to corrosion potential, Ecorr. Before polarizing the samples or performing actual corrosion tests, the open circuit potential (OCP) stability was ensured. Stability was generally observed after 1 hour, and actual polarization can occur in about 15 minutes. All experiments were performed at ambient temperature. After

testing, the corrosion current density, i_{corr} was obtained by extrapolating the linear portion of the software-generated potentiodynamic polarization plot to E_{corr}.
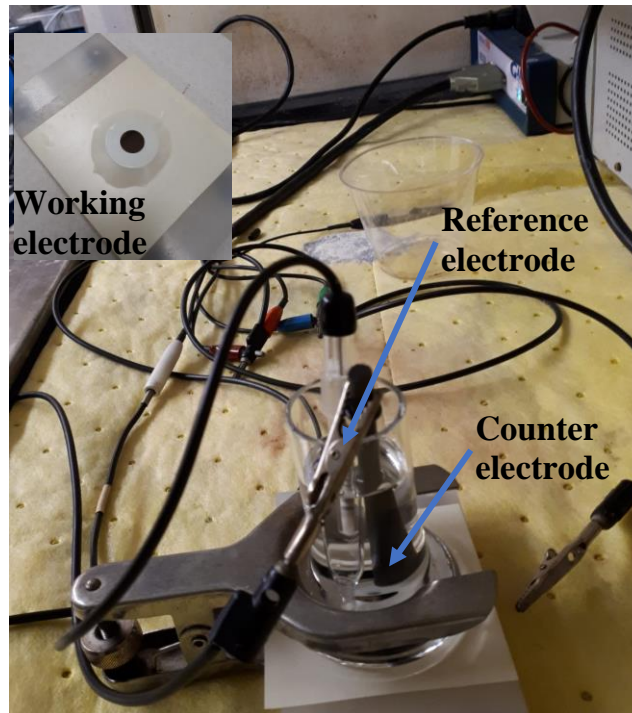
Figure 3.4. Potentiodynamic test set-up

CHAPTER 4

RESULTS AND DISCUSSION

4.1 Effect of Nb target power on the composition and structure of Nb-DLC films

4.1.1 X-ray Photoelectron Spectroscopy (XPS)

4.1.1.1 Elemental composition

XPS was used to analyze the chemical composition and chemical state of Nb and C in the films. XPS survey spectra of a Nb-DLC film deposited at 40 W power on Nb target is presented in Figure 4.1. It shows the oxygen content on the surface is much higher than that of the subsurface after 5 minutes of etching. Similar phenomena were observed for all Nb-DLC films. However, the undoped DLC films show little amount of oxygen, indicating that a thin Nb oxide layer form on the top surface of the Nb-DLC films. This layer is probably formed due to air exposure. Results similar to this have been reported in sputtered Nb-doped DLC and niobium carbide films [5,15,62]. Figure 4.2 shows the XPS survey spectra for all samples (after 3 min sputtering etching), and C 1s, Nb 3d, and O 1s core level peaks are detected in all the Nb-DLC films. In addition, Nb 3s and Nb 3p peaks are also present. However, for the undoped DLC film, only C 1s and O 1s is observed as expected.

Figure 4.3 shows the average composition of elements at the subsurface of the films based on XPS analyses. This concentration was calculated from the area and sensitivity factor of Nb 3d (Relative Sensitivity Factor, (RSF) = 2.92), C 1s (RSF = 1.0), and O 1s (RSF = 0.78) peaks. Nb 3d peak is generally considered for analysis because it is the primary or core level XPS peak for Nb. The results show that the films consist of mainly carbon and Nb with a minute amount of oxygen. The concentration of carbon in the films ranges from 99.96 at. % to 73.32 at. % and the concentration of niobium ranges from 0 to 24 at. % when the Nb target power increases from 0 to 50 W.

26
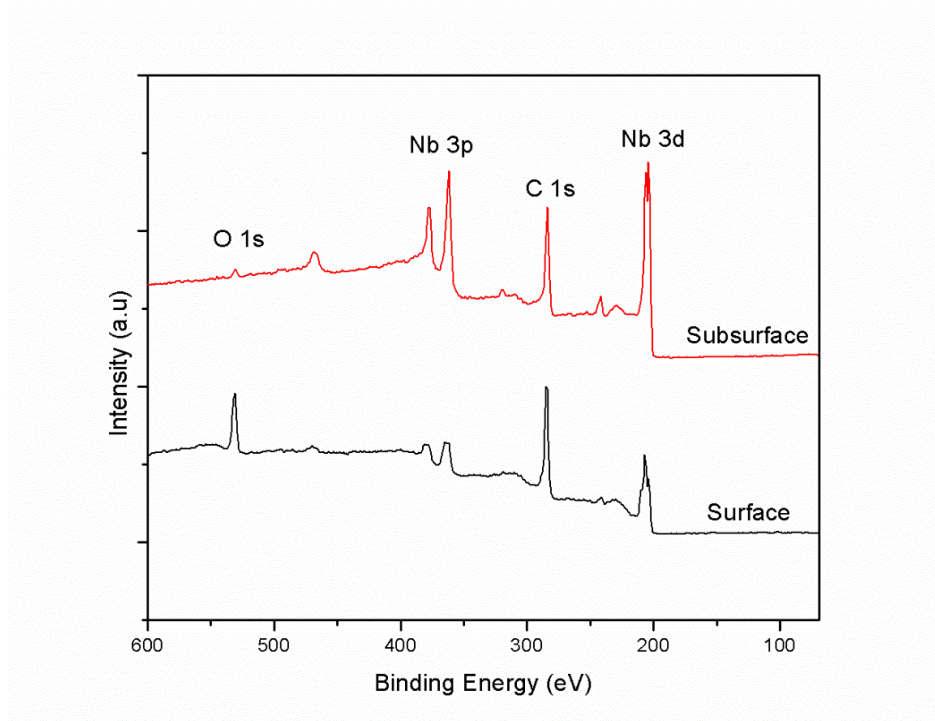
Figure 4.1. XPS survey scans of Nb-DLC 40 W showing oxidation at the surface of an Nb-DLC film.
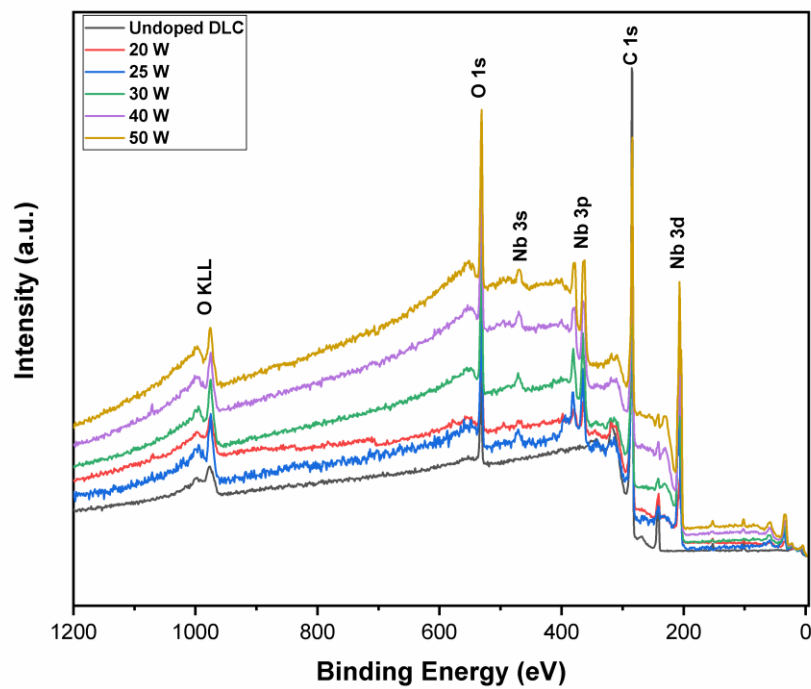
Figure 4.2. XPS full spectra of the films deposited with different Nb target powers.
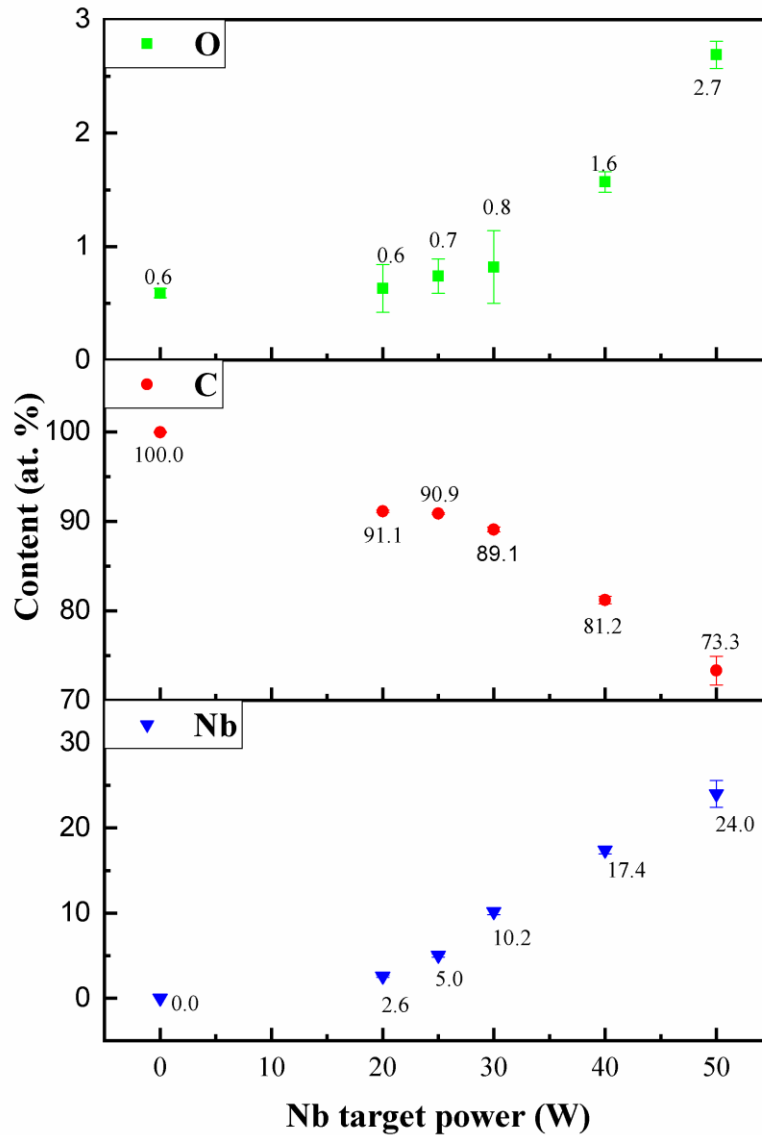
Figure 4.3. Subsurface composition of the films deposited at different Nb target power.

4.1.1.2 The bonding states of niobium and carbon

The detailed chemical states of elements in the DLC and Nb-DLC films were investigated using the XPS. The resulting C 1s spectra as a function of Nb target powers are presented in Figure 4.4. The presence of carbide and the relative amounts of sp^3 to sp^2 carbon hybridization in the films could be verified from these results. These spectra can be deconvoluted into three or four Gaussian

peaks: C-C (sp^3), C=C (sp^2), C-Nb and C-O/C=O which corresponds approximately to binding energies of 285.2, 284.4, 283 and 286-288 eV, respectively [8,48,63]. The DLC and Nb-DLC films deposited at 20 W and 25 W could only be deconvoluted with three peaks. Also, the Nb-DLC films synthesized at 30 W, 40 W, and 50 W could be fitted with four peaks. It is observed that the chemical states of carbon changed with various Nb contents. A summary of these states is presented in Table 4.1.
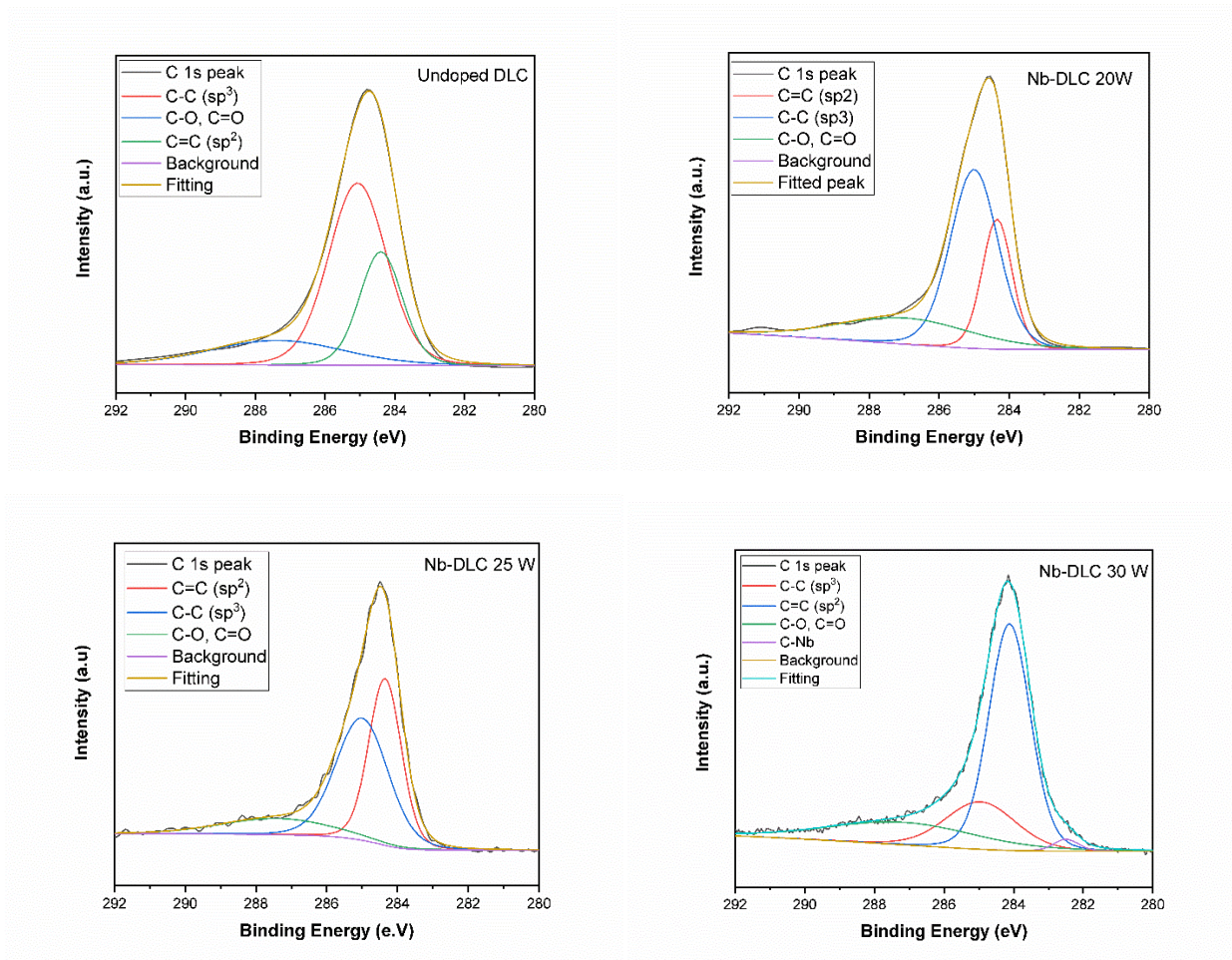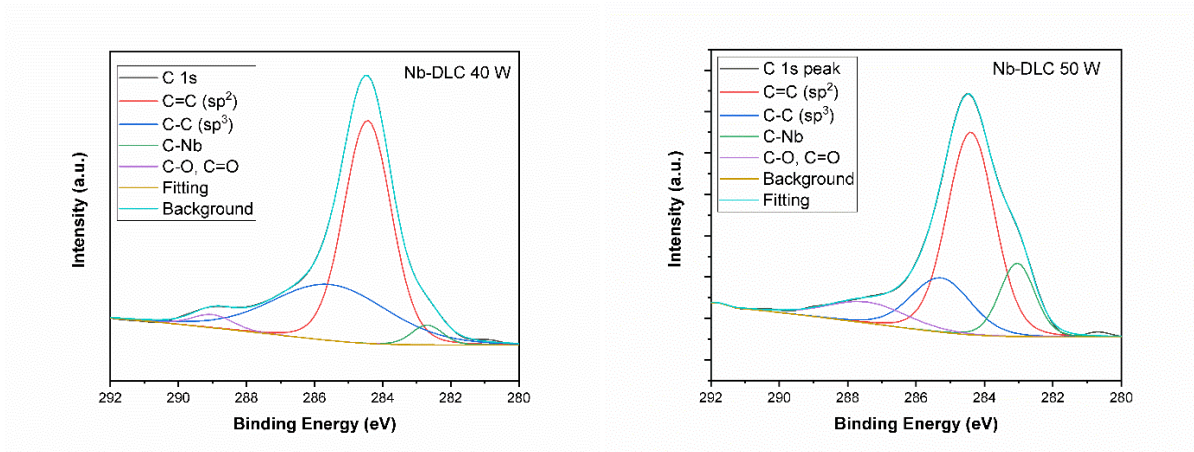
Figure 4.4. High resolution XPS spectra for C1s.

Table 4.1. Summary of the chemical states of carbon in the films.

Core level	Film	Chemical state	Binding Energy (eV)	sp^3 %
C1s	DLC	C-C (sp^3)	285.07	57.9
		C=C sp^2	284.40	
		C-O, C=O	287.38	
	Nb-DLC 20 W	C-C (sp^3)	285.00	53.5
		C=C sp^2	284.35	
		C-O, C=O	286.95	
	Nb-DLC 25 W	C-C (sp^3)	285.01	46.9
		C=C sp^2	284.44	
		C-O, C=O	287.31	
	Nb-DLC 30 W	C-C (sp^3)	285.24	23.9
		C=C sp^2	284.41	
		C-O, C=O	287.18	
		C-Nb	282.80	
	Nb-DLC 40 W	C-C (sp^3)	285.28	18.9
		C=C sp^2	284.40	
		C-O, C=O	287.43	
		C-Nb	283.04	
	Nb-DLC 50 W	C-C (sp^3)	285.57	17.1

C=C sp^2	284.44
C-O, C=O	289.00
C-Nb	282.69

As the amount of Nb in the films increases from 0 – 24 at. %, the structure of the films changes from an amorphous carbon structure to a composite structure with carbide embedded in the amorphous matrix as seen in the films containing 10.2, 17.4, and 24.0 at. % where C-Nb bonds have been observed. C 1s binding energy as C-Nb chemical state is found to be around 283 eV, similar to that reported by Ding et al. [8]. This peak, at 283 eV, was not found in the films with Nb concentration less than 10.2 at. %, which indicates the Nb incorporated into the carbon matrix does not bond with the carbon atoms. Also, it is observed that increasing Nb concentration results in a decrease in sp^3 carbon bond and an increase in sp^2-C bond, which implies that the incorporation of Nb promotes carbon graphitic carbon phase.

The Nb 3d core level spectra for all the Nb-DLC films are presented in Figure 4.5. A peak around 204 eV that corresponds to Nb 3d$_{5/2}$ for Nb-C bonding [8,18] and another one around 207 eV for Nb-O were observed, suggesting the formation of Nb carbides and oxides. Additionally, the intensity of the Nb 3d peak increases with the increase of Nb target power. The spectra could be deconvoluted or fitted into 5 peaks, as shown in Figure 4.6 (for Nb-DLC at 50 W). A summary of the chemical states of Nb, including the full width half maximum (FWHM) and their binding energies [8,64] are presented in Table 4.2, which agree well with the reported results [8,64]. In previous studies on Nb-based materials, several chemical states such as Nb-Nb (~202.2 eV), Nb–C (~203.7 eV), Nb–O bonds (202.9–207.6 eV), and oxycarbide NbC$_x$O$_y$ (204.4–205.8 eV), can be obtained [64,65]. Due to the unavoidable overlap seen in the bond energies, it has been accepted that fitting these spectra has some difficulty [64]. In the Nb-doped films deposited in this investigation, Nb-Nb bonds were not observed.
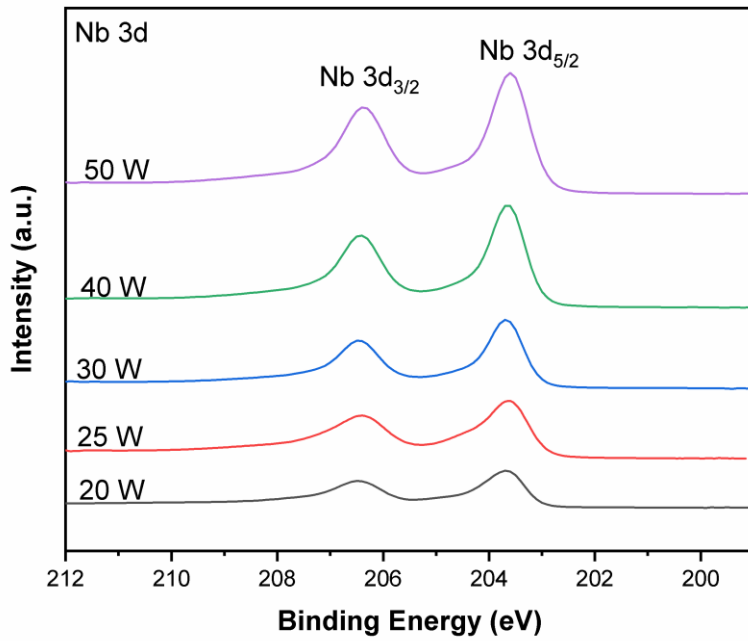
Figure 4.5. Nb 3d XPS spectra of Nb-DLC films with different Nb contents
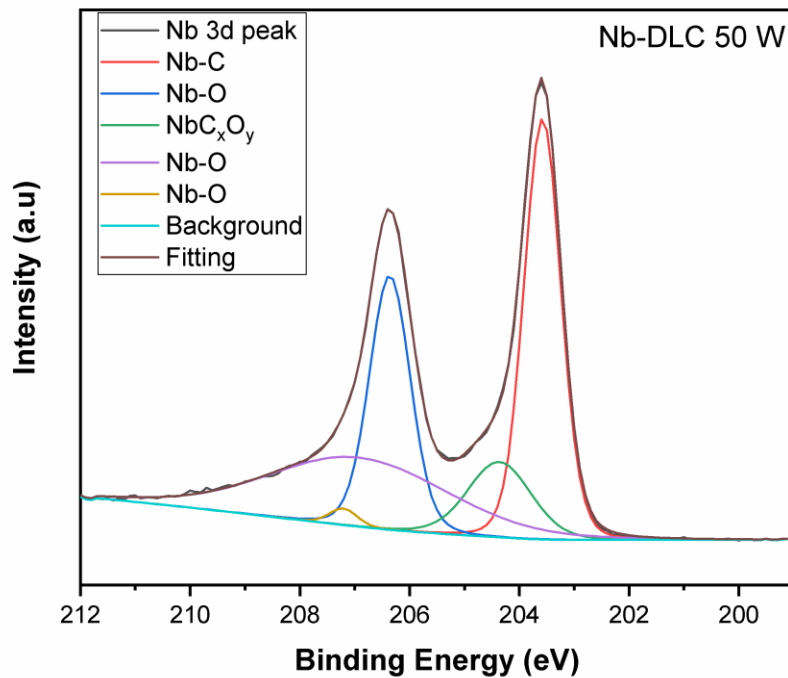
Figure 4.6. Deconvoluted Nb 3d XPS spectrum of the Nb-DLC 50 W film

Table 4.2. Summary of the chemical states of Nb in the films.

Nb power (W)		Chemical states				
		Nb-C	NbC$_x$O$_y$, Nb-O	Nb-O	Nb-O	Nb-O
50	Position	203.58	204.36	206.36	206.94	207.21
	FWHM	0.8	1.4	0.9	3.9	0.6
	Area	11567	3552	7780	9224	345
	% conc.	35.8	11.0	23.9	28.3	1.1
40	Position	203.62	204.28	206.41	206.79	207.15
	FWHM	0.7	1.2	0.8	3.8	0.8
	Area	8781	3000	5732	8350	395
	% conc.	33.6	11.5	21.8	31.7	1.5
30	Position	203.66	204.28	206.44	206.82	207.18
	FWHM	0.7	1.2	0.8	3.9	0.9
	Area	5636	2258	3674	5931	360
	% conc.	31.7	12.7	20.5	33.1	2.0
25	Position	203.57	204.22	206.36	206.96	207.09
	FWHM	0.8	1.3	0.9	4.0	0.9
	Area	4631	3444	3407	6953	675
	% conc.	24.3	18.0	17.8	36.4	3.5
20	Position	203.54	204.37	206.17	206.93	207.34
	FWHM	0.8	1.3	1.1	2.2	0.8
	Area	1676	1457	2229	2116	701
	% conc.	14.1	17.0	19.0	17.6	17.6

4.1.2 Raman spectroscopy

The Raman spectra showing the bonding state of carbon in the DLC and Nb-DLC films are presented in Figures 4.7. The spectra were deconvoluted into D and G bands of carbon using two Gaussian curves. When DLC films are doped with metals, the band positions, the full width half maximum (FWHM) of the bands, and the intensity ratio of the D peak to G peak (I_D/I_G) might change and can be used to evaluate the structure of the films. The characteristics of the bands in the films are summarized in Table 4.3.

In general, when DLC films are doped with metals, the I_D/I_G ratio increases with the increase of doping amount of metals [16,50,52,66,67]. This characteristic trend was observed for the Nb-DLC

films synthesized in this investigation [16,50,52,66,67] This increase usually imply a reduction in sp^3/sp^2 bonding ratio or an increase in sp^2/sp^3 bonding ratio, and is attributed to a higher disorder of carbons in the films [16]. Increase in sp^2 bonds implies more graphitic carbon and often results in a decrease in hardness. In some instances, it has been found that the sp^3/sp^2 ratio increases when the doping level of metals is very low, which often translated to better hardness compared to that of undoped DLC [48,68].

Asides from the I_D/I_G ratio, which is mostly used, the shift in the G band is also used to understand the film bonding structure. In this study, the G band position moves slightly to a higher wavelength when the doped metal content increases. A similar trend was observed previously [52,66]. The shift can be attributed to the increase in the size of sp^2-C clusters.
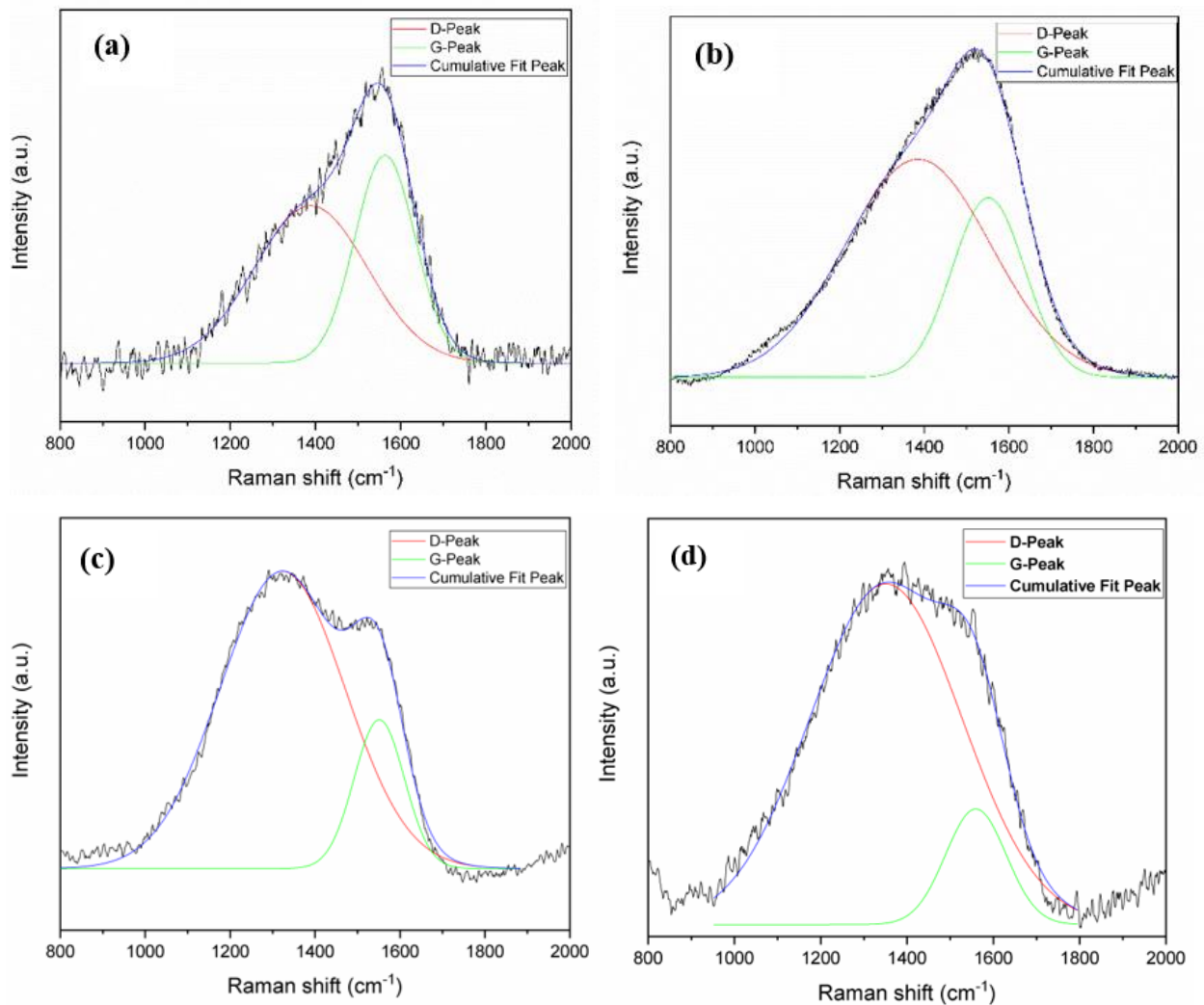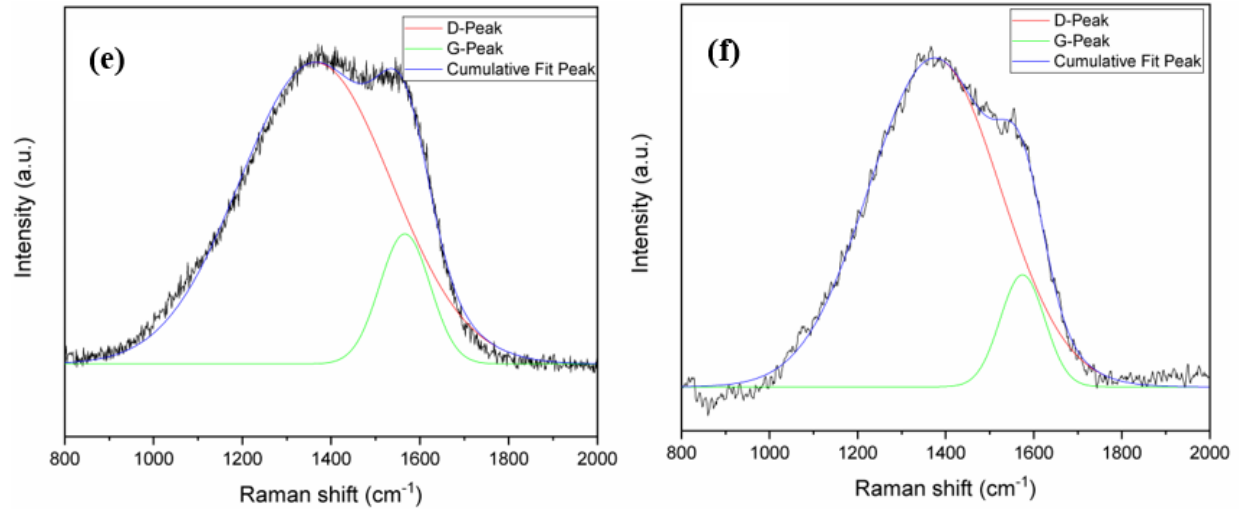
Figure 4.7. Gaussian fitting of DLC and Nb-DLC films with different doped Nb contents (a) 0 at. %, (b) 2.6 at. %, (c) 5.0 at. %, (d) 10.2 at. %, (e) 17.4 at. %, (f) 24.0 at. %

Table 4.3. Summary of Raman analysis showing I_D/I_G G-Position and G_{FWHM}

Figure	Nb Target Power (W)	Nb content (at. %)	I_D/I_G	G-Position (cm^{-1})	G_{FWHM} (cm^{-1})
a	0	0	0.5	1549.0	204.8
b	20	2.6	0.9	1549.4	187.5
c	25	5.0	1.8	1540.9	167.1
d	30	10.2	1.9	1550.1	151.1
e	40	17.4	1.9	1557.5	143.3
f	50	24.0	2.4	1559.6	111.6

4.1.3 X-ray Diffraction (XRD)

The Nb interlayers deposited at 73 and 163 V were analyzed with grazing incidence XRD. The XRD diffractograms are shown in Figure 4.8. All the peaks match with Nb peaks and are broadened, indicating that Nb is present as nanocrystallites. The crystallographic (hkl) orientations of these Nb peaks after matching with the reference pattern (00-034-0370) are (110), (200), (211), (220) for the peaks at 38.48°, 55.54°, 69.59° and 82.45°, respectively. The other peaks at 43.78°, 46.77°, and 50.90° are from CoCrMo substrate.

35

Ti and Cr metals are commonly used to improve the adhesion of DLC films. From the finite element analysis of Wei et al. [69], the selection of an interlayer material should be based on its coefficient of thermal expansion, which should lie in between that of the substrate and film. Nb meets this criterion as seen in Table 4.4, and it was used as an interlayer between stainless steel and Nb-DLC by Ding et al. [8].

Table 4.4. Material properties of Nb, CoCrMo and DLC

Material	Young's Modulus (GPa)	Poisson's ratio	Yield stress (MPa)	Thermal coefficient of expansion (µm/m K)	Ref.
CoCrMo	210	0.29	450	12	[70]
Si	164.4	0.224	4410	3.2	[69]
Nb	104.9	0.397	240 - 550	7.2	[71]
DLC	120	0.25	4610	2.3	[69]
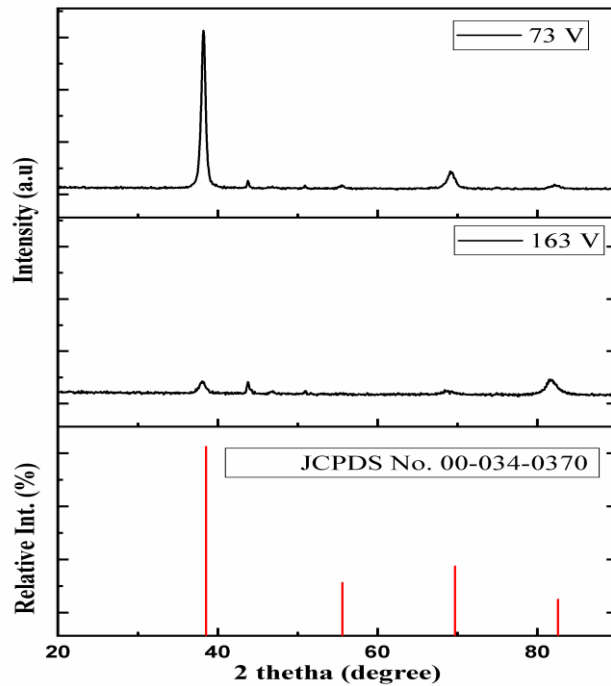
Figure 4.8. Grazing incidence XRD θ-2θ scan of Nb films deposited on CoCrMo substrate at different bias voltages.

The Nb-DLC films were prepared on Si and CoCrMo substrates with a Nb interlayer. The grazing incidence XRD patterns showing the evolved phases in these films as a function of Nb target powers are presented in Figure 4.9. The observed film peaks are similar for both substrates. The peaks are summarized in Table 4.5. Although a low grazing incidence angle of 3° was used to minimize the contribution from the substrate, it is observed that peaks from the substrate appear in all the samples, indicating that the Nb-DLC films are thin.
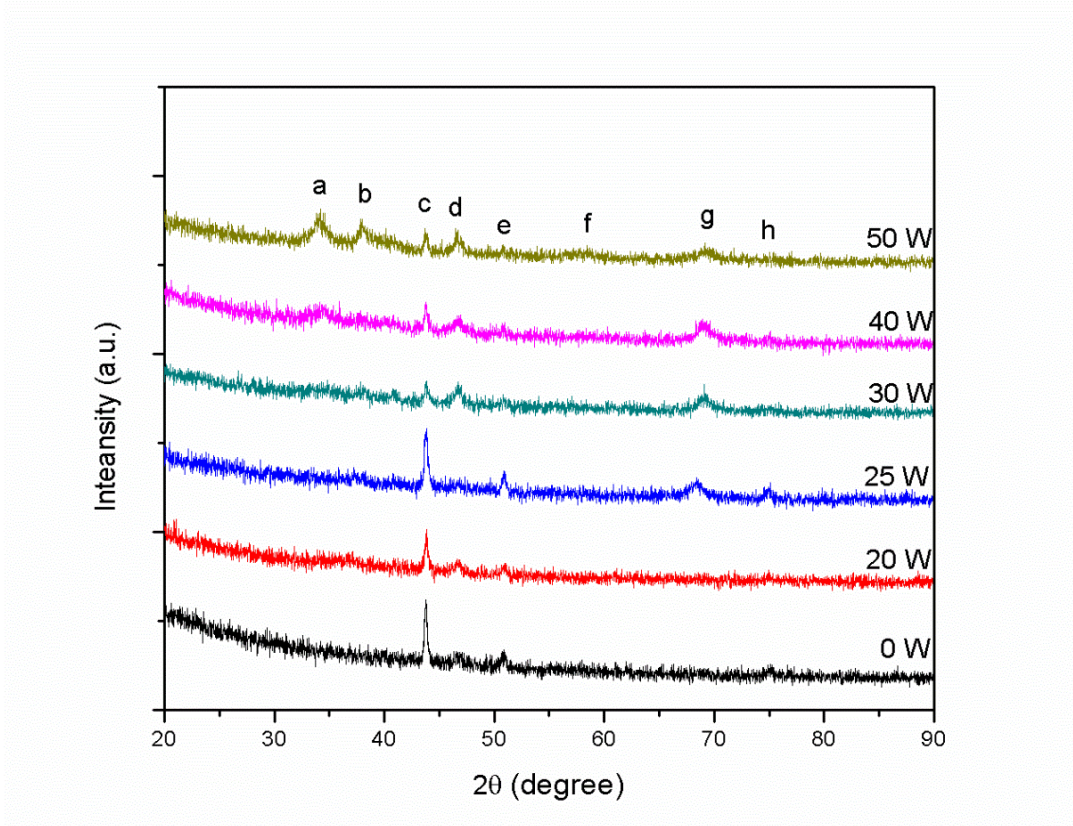
Figure 4.9. Grazing incidence XRD θ-2θ scan of Nb-DLC films deposited on CoCrMo substrate at different target powers.

Table 4.5. Peak summary for the DLC and Nb-DLC films

Peaks	2-theta position	Identified peaks(hkl)
a	34.04	NbC(111)
b	37.9786	$Nb_2C(211)$
c	43.7429	Substrate
d	46.6667	Nb_2O_5
e	51.1112	Substrate
f	57.7211	NbC(220)
g	69.2621	Nb(211), NbC(311)
h	74.9625	Substrate

Graphitic carbon or diamond peaks were not detected for all the samples, signifying that the carbon in all the films is of amorphous nature. The undoped DLC film shows no peaks and consists of amorphous carbon. For the film deposited at 20 W Nb target power, the XRD pattern is similar to that of the undoped DLC, indicating that the doped Nb may be dissolved into the DLC amorphous matrix rather than form a second phase. Similar results were reported previously [8,50,51,66]. However, as the Nb target power increases, Nb began to bond with carbon to form Nb-C phases. Initially, NbC phase forms but upon reaching the Nb target power of 50 W (when Nb content is 24.0 at. %), a combination of NbC and Nb_2C nanocluster are obtained.

The XRD results imply that Nb atoms could dissolve into the DLC matrix at a low concentration to form an amorphous structure. However, with further incorporation of Nb, the formation of Nb-C nanocrystallites to form nanocomposite structure is likely. Similar phase evolution was reported for Nb-doped DLC films reported elsewhere [7,8].

4.2 Effect of target power on mechanical properties of the films

4.2.1 Hardness and Elastic Modulus

The films' hardness is an important mechanical property that depicts their reliability and durability. When metals are incorporated into DLC, hardness is generally reduced except in few cases which has been reported in the literature. In this study, the hardness and elastic modulus of the Nb-DLC films with different Nb contents were measured, and the summary of the results is presented in

Figure 4.10. As shown in the table, the hardness and Young's Modulus of the undoped DLC film is 24 and 201 GPa, respectively. As the Nb content increases from 0 to 24 at. %, the hardness drops from 24 GPa to 11.6 GPa. When the Nb amount is not over 5.0 at. % (Nb-DLC 25 W), the hardness values for the films are close to that of the DLC films. Reduction in hardness can be attributed to the decrease of sp^3 C-C bonds in the films [7] and the formation of Nb-C (as seen from the XRD and XPS results), which may break the continuity and integrity of the carbon network structure [48,53]. [7]. It can be seen from Table 4.4 that sp^3 bond is reduced with the increase of Nb content. It is also observed that the hardness trend is not to the elastic modulus, which has also been reported previously [41,48,53]. Lastly and importantly, the hardness values of all the films are higher than that of CoCrMo substrate (8.0 ± 0.4 GPa).
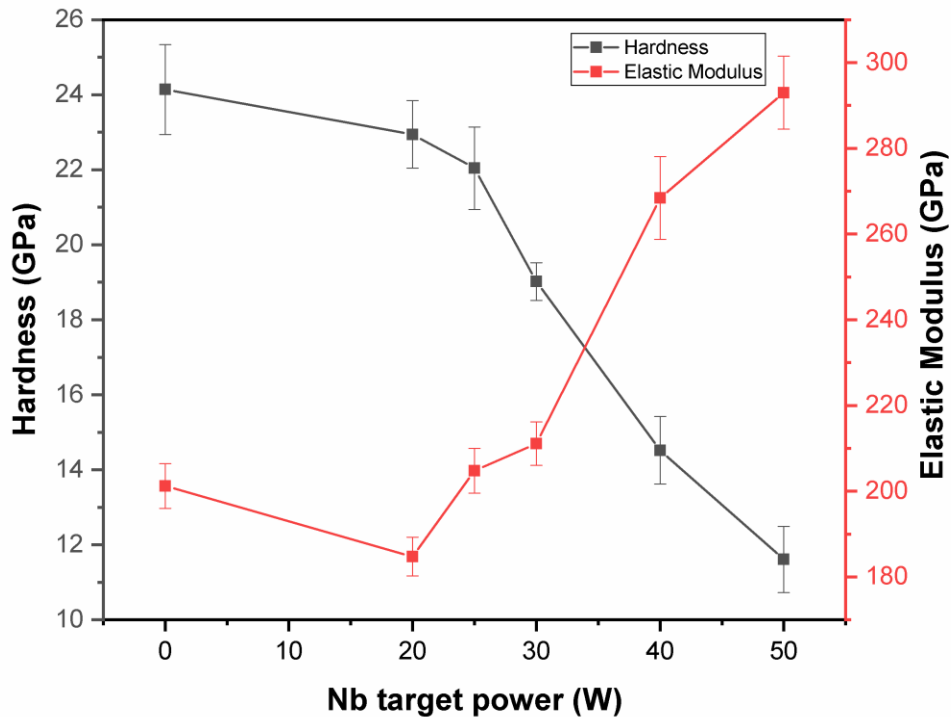

Figure 4.10. Hardness and elastic modulus of DLC and Nb-DLC films

Also, the ratio of hardness (H) to elastic modulus (E), H/E and H^3/E^2 is calculated and presented in Table 4.6. The H/E ratio corresponds to the film's elastic strain to failure while the H^3/E^2 ratio is directly related to the elastic-plastic behavior of the films [72]. It can be seen that the H/E and

H^3/E^2 of the Nb-DC film with 2.6 at% Nb are the highest among all the Nb-DLC film, indicating the film might possess the best wear resistance [41].

4.2.2 Internal (compressive) stress

High compressive stresses reaching about 10 GPa may be developed in DLC films thereby affecting their adhesion to metallic substrates, thus limiting their industrial applications [40,73]. It was also stated in a review article by Love et al. [54] that those stresses should be less than 1 GPa to avoid delamination and catastrophic failure. The evolution of internal stress with niobium doping is presented in Figure 4.11. The stresses in the Nb-doped DLC films are lower than 1 GPa, and much lower than that in the undoped DLC films. This implies that Nb doping is effective in reducing the internal stress in DLC films. A significantly reduced compressive stress was observed in the film with the minimal amount of 2.6 at. % of Nb. The reduction in stress could be attributed to several factors. Firstly, the incorporation of Nb results in clusters that relax the distorted bonds and lengths, therefore reducing compressive stress [8,48]. Secondly, Nb doping reduces the amount of sp^3 carbon bonding in the film as a result of ion bombardment during deposition [40]. After the sharp drop at 2.6 at. %, further increase in Nb content results in an increase in stress, although all the stresses are still below that of the undoped film. A similar trend whereby stress initially reduces, then increases with metal concentration, has been reported in the experimental works involving different metal dopants [74]. This kind of behavior was further proven in a study where molecular dynamics simulation was used to model the residual stress of DLC films when doped with Ti, V, Cr, Zr, Nb and W metals [75].
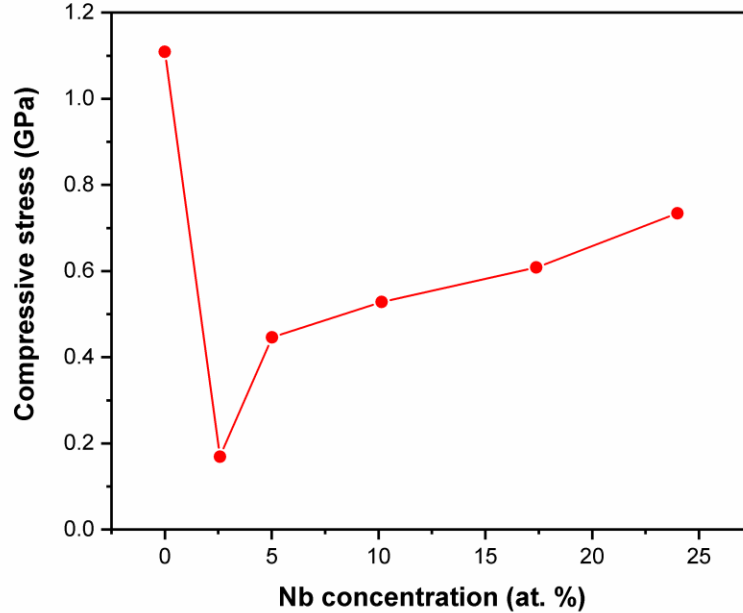
Figure 4.11. Internal stress as a function of Nb content

Table 4.6. Hardness and elastic modulus of the Nb-DLC films

Nb target power (W)	Nb content (at. %)	H (GPa)	E (GPa)	H/E	H^3/E^2
0	0	24.1 ± 1.2	201.2 ± 5.2	0.12	0.35
20	2.6	22.9 ± 0.9	184.7 ± 4.6	0.12	0.35
25	5.0	22.0 ± 1.1	204.8 ± 5.2	0.11	0.26
30	10.2	19.0 ± 0.6	211.1 ± 5.1	0.09	0.15
40	17.4	14.5 ± 0.9	268.4 ± 9.7	0.05	0.04
50	24.0	11.6 ± 0.9	293.0 ± 8.5	0.04	0.02

4.2.3 Adhesion strength

Besides hardness, the film's adhesion to the substrate is another critical property determining its performance. The SEM images of the impressions made on the films after Rockwell C indentation tests are presented in Figure 4.12. Compared with the VDI standard, it is observed that all the films exhibited good adhesion strength as no delamination or spallation was observed. However, for the samples deposited at 40 and 50 W Nb target power, radial cracks developed. Similar radial cracks

obtained for niobium nitride (NbN) coatings deposited using cathodic arc PVD were said to provide sufficient adhesion [76].
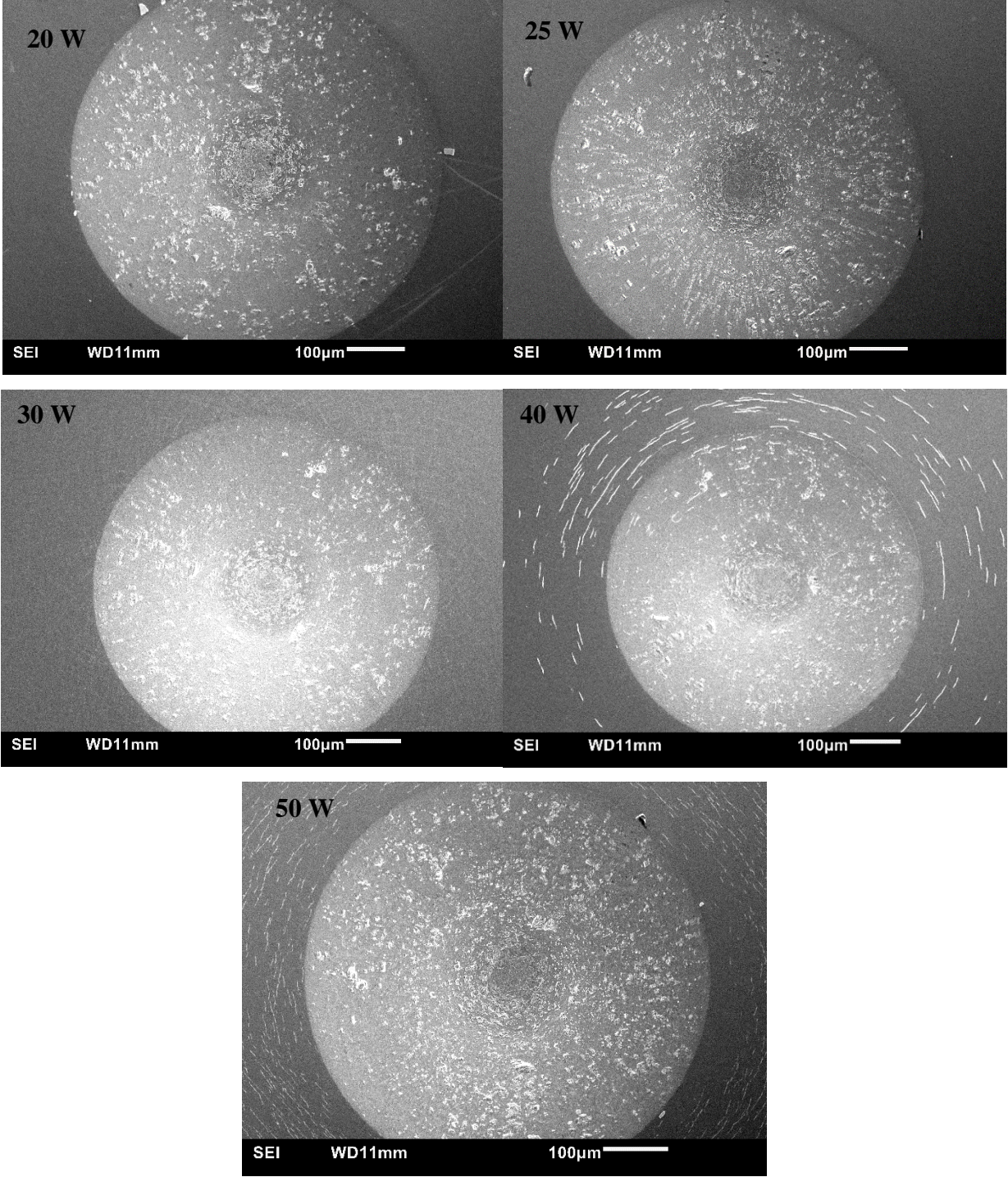
Figure 4.12. SEM images of the Rockwell Indentation of the Nb-DLC films

4.3 Effect of target power on the tribological behavior of the films

4.3.1 Coefficient of friction

Presented in Figure 4.13 is a plot of the coefficient of friction (COF) of the CoCrMo alloy substrate, undoped DLC, and Nb-DLC films versus time. The specimens were sliding linearly against UHMWPE counterpart pins in a pin-on-disc tribometer under a constant load of 10 N for 10000 seconds in a reciprocating mode. From the plot, it can be observed that COF decreases from 0.22 for CoCrMo alloy to 0.15 for Nb-DLC with 2.6 at. %. The undoped DLC and low-doped DLC can reduce the friction coefficient of CoCrMo alloy. Generally, it is challenging to compare friction and wear results with published data due to a significant difference in testing conditions. Nonetheless, the COF for CoCrMo in this investigation was similar to that of Huang et al. under similar conditions [2]. Also, DLC-coated CoCrMo alloy has been reported to reduce COF of CoCrMo alloy [77]. Further incorporation of a higher amount of Nb atoms above 2.6 at. % results in a gradual increase of COF up to 0.35. The increase of COF of Nb-DLC films may be attributed to the increase of niobium carbide and wear debris generated when sliding against the polymeric pins.

4.3.2 Wear

The wear rates of UHMWPE pins, CoCrMo alloy, undoped DLC and Nb-doped DLC films are summarized in Table 4.7. The uncoated (CoCrMo) alloy caused the most severe wear to the pin as observed from the wear rate of 4.20E-03. With DLC film, this reduced by more than 2-fold. However, it was observed that all the Nb-doped DLC films reduced the wear of the polymer films, which presents a potential to reduce osteolysis. Most significantly, no measurable wear to the pin was observed when the least doped DLC film was sliding against it. For the films, it was observed that with an increase in Nb content, the wear rate of Nb-DLC increases. Although, it is important to note that there was no visible wear to other films. It is seen that the film with the least amount of Nb had the most outstanding tribological behavior, and this can be corroborated by the higher H/E and H^3/E^2 ratio in table 4.9. Figure 4.14 shows the wear tracks of Nb-DLC films containing 17.4 and 24.0 at. % Nb, which displays wear of the films.
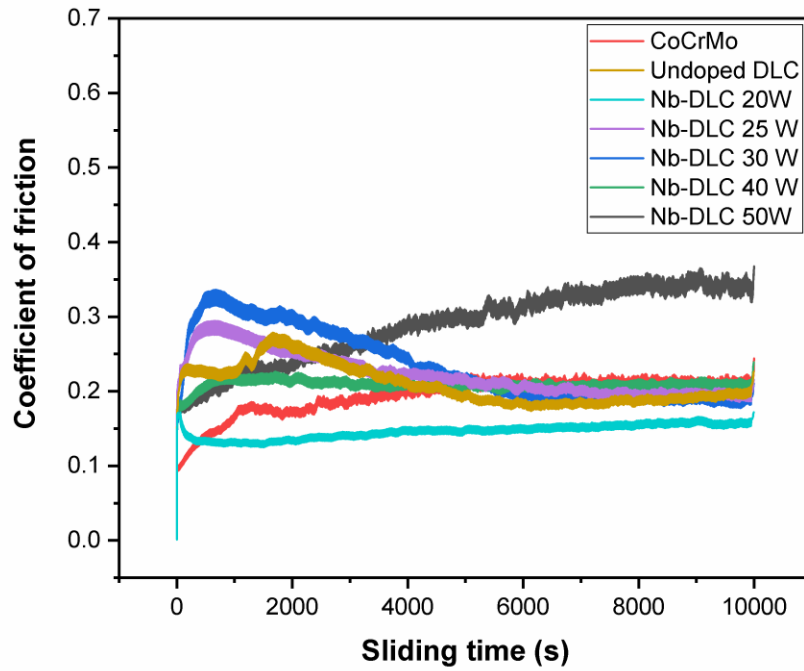
Figure 4.13. Coefficient of friction as a function of sliding time for all specimens

Table 4.7. Wear and friction results of the coated and untreated specimens.

Nb content (at. %)	Sample	Pin wear volume (mm^3)	Film wear volume (mm^3)	Wear rate of pin (mm^3/N*m)	Wear rate of film (mm^3/N*m)	COF
	CoCrMo	10.498	-	4.20E-03	No wear	0.22
0	DLC	3.105	0.00001	1.27E-03	4.00E-09	0.18
2.6		0.000	-	0.00E+00	No wear	0.15
5.0		0.159	-	6.36E-05	No wear	0.19
10.2	Nb-DLC	0.477	-	1.91E-04	No wear/Very low	0.19
17.4		0.636	0.029685	2.55E-04	1.19E-05	0.21
24.0		1.591	0.064695	6.36E-04	2.59E-05	0.35

Figure 4.14. Optical image of wear track Nb-DLC films with 17.4 at. % Nb (left) and 24.0 at. % Nb (right)

4.4 Effect of target power on the corrosion behavior of the films

The potentiodynamic polarization curves of CoCrMo substrate alloy, undoped DLC, and Nb-DLC samples in 0.9% (w/v) NaCl are presented in Figure 4.15. Also, the corrosion potential (E_{corr}) and corrosion current density (i_{corr}) as a function of Nb content are summarized in Table 4.8. The corrosion current density, which indicates the sample's corrosion resistance, was obtained by extrapolating the linear portions of the anodic and cathodic branches of the polarization curves. Generally, lower i_{corr} values indicate higher corrosion resistance. In this study, the DLC film provides better corrosion resistance than the uncoated substrate since its corrosion current density (3.6 nA/cm^2) is about six times lower than that of CoCrMo alloy (19.2 nA/cm^2). When 2.6 at. % Nb is present in the DLC matrix, the corrosion resistance is increased by only 6 % compared to the undoped DLC. This may be attributed to the similarities in their structures as seen in the XRD and XPS results. A further increase of Nb content to 5.0 at. % results in an increase of corrosion resistance by 92 % and 59 % compared to CoCrMo and undoped DLC film, respectively. This improvement may be due to niobium's good corrosion resistant property. However, it was observed that the increase in Nb content beyond this led to a gradual but slight decrease in corrosion resistance. This trend is in good agreement with niobium carbide films deposited by Braic et al. [78]. Lastly, the E_{corr} is thermodynamic value which simply indicates the possibility of corrosion resistance. Generally, this parameter is not as important as the i_{corr}, however a higher

value may indicate better corrosion resistance. It was observed that the lowest i_{corr} corresponds to the highest positive E_{corr}.
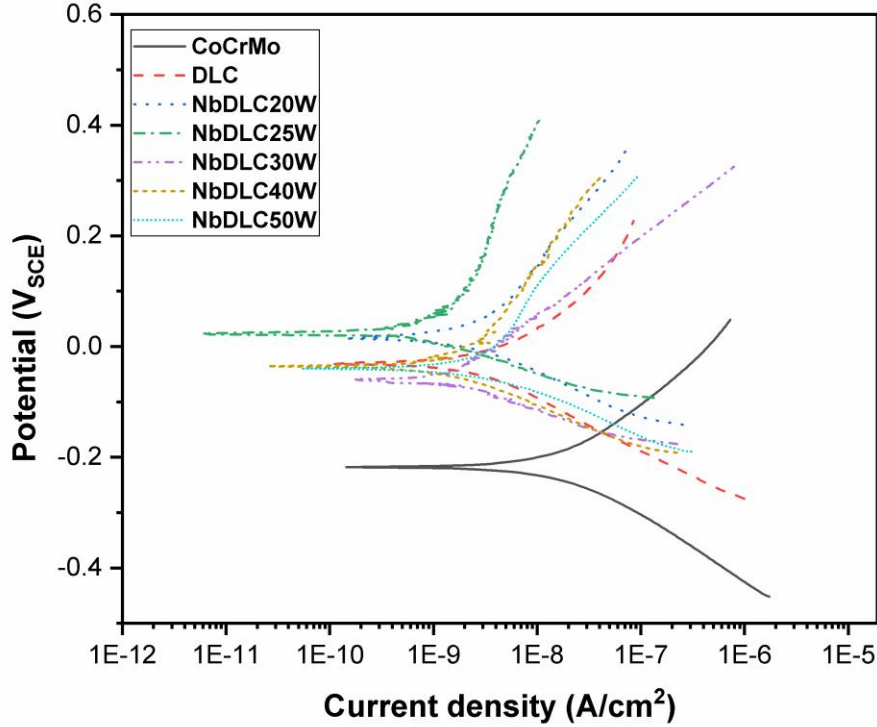
Figure 4.15. Potentiodynamic polarization curves of the CoCrMo substrate alloy, undoped DLC and Nb-DLC samples

Table 4.8. Results of potentiodynamic polarization studies of CoCrMo substrate alloy, undoped DLC and Nb-DLC samples.

Specimen	Nb content (at. %)	E_{corr} (mV)	i_{corr} (nA/cm^2)	~Protective efficiency (%)
CoCrMo		-217.0	19.2	
Undoped	0	-39.7	3.6	81
20 W	2.6	15.1	3.4	82
25 W	5.0	22.8	1.47	92
30 W	10.2	-60.2	1.56	92
40 W	17.4	-39.0	2.16	89
50 W	24.0	-34.3	2.88	85

CHAPTER 5

SUMMARY, CONCLUSIONS, AND RECOMMENDATION

5.1 Summary and conclusions

In this thesis, DLC and Nb-doped DLC films were prepared on Si and CoCrMo substrates using radio frequency magnetron sputtering technique. The amount of Nb in the films was varied between 2.5 and 24.0 at. %, and its effect on structure, mechanical, tribological and corrosion performance was examined. The films containing a lower amount of Nb showed the best properties. The main results and conclusions are detailed below:

- Compositional analysis showed that an increase in Nb rf target power resulted in a corresponding increase in Nb content as well as surface adsorbed oxygen in the DLC films. Also, the maximum solubility of Nb atoms in the films occurred when the Nb content was 2.5 at. %.

- Structural characterization shows that a further increase in Nb content beyond 2.5 at. % up to 24.0 at. %, resulting in the transformation of the amorphous structure of DLC to a composite structure. This is evident from XRD results showing crystalline NbC and Nb_2C phases embedding in the DLC matrix. XPS results further confirm the existence of Nb-C bonds in Nb-DLC and show that the incorporation of Nb atoms results in reduction of sp^3 bonded carbon.

- Although the hardness of the films reduces with the increase of Nb amount, the compressive stresses could be greatly reduced by controlling Nb content. At low content of 2.5 at. % of Nb, there was a 5 % decrease in hardness compared to the undoped DLC. However, the compressive stress was reduced by 85 %, indicating Nb doping can greatly reduce the stresses with only an insignificant reduction in the hardness.

- For tribological performance, the Nb-DLC films were able to reduce wear volume and consequently the rate of wear of the UHMWPE pins, an indication that Nb doping may be able to reduce the possibility of osteolysis and extend implant life. Also, low amount Nb doping is able to reduce the friction coefficient.

- As compared to the CoCrMo substrate alloy, all the films exhibited superior corrosion behavior in NaCl solution. The best corrosion resistance (i_{corr} = 1.47 nA/cm^2) and

47

protective efficiency ($\sim$ 92 %) was observed for Nb-DLC with a low amount Nb (5.0 at. %).

5.2 Recommendations for future works

The following recommendations for future works based on the outcomes of this study is presented below:

1. It is recommended to investigate the effect of Nb amount (less than 2.6 at%) on the structure and performance of Nb-doped DLC films.
2. It would be beneficial to investigate the Nb-DLC films for their toxicity, cellular adhesion, proliferation, and viability, even though Nb was reported to be biocompatible.
3. Further tribological and corrosion testing, or tribo-corrosion testing in fluids that simulates the body conditions, is recommended to verify the applicability of these films for joint applications.
4. It is recommended to investigate the structure and homogeneity of Nb-DLC films using transmission electron microscopy to understand the nature Nb in the films.
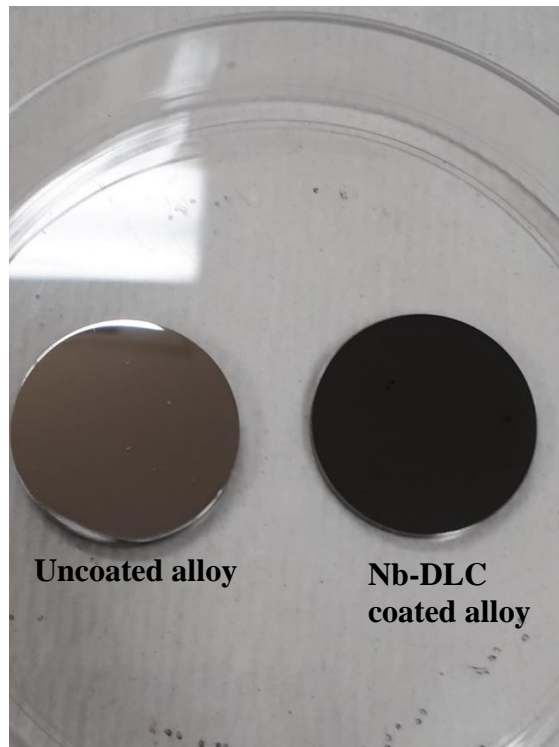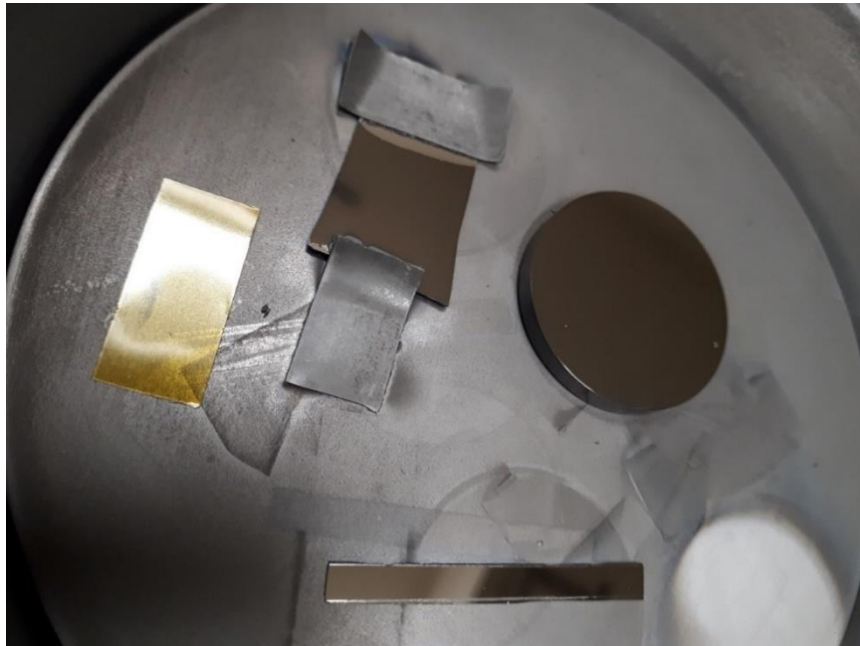
APPENDIX

Figure A.1. Bare alloy and coated alloy

REFERENCES

[1]   M.T. Mohammed, Nanocomposites in total hip joint replacements, Elsevier Inc., 2018. doi:10.1016/B978-0-12-813740-6.00012-0.

[2]   P. Huang, A. Salinas-Rodriguez, H.F. López, Tribological behaviour of cast and wrought Co–Cr–Mo implant alloys, Mater. Sci. Technol. ISSN. 15 (1999) 1324–1330. doi:10.1179/026708399101505284.

[3]   K. Zhang, M. Wen, G. Cheng, X. Li, Q.N. Meng, J.S. Lian, W.T. Zheng, Reactive magnetron sputtering deposition and characterization of niobium carbide films, Vacuum. 99 (2014) 233–241. doi:10.1016/j.vacuum.2013.06.012.

[4]   M.G. di V. Cuppari, S.F. Santos, Physical properties of the NbC carbide, Metals (Basel). 6 (2016) 1–17. doi:10.3390/met6100250.

[5]   L. Yate, L.E. Coy, D. Gregurec, W. Aperador, S.E. Moya, G. Wang, Nb-C nanocomposite films with enhanced biocompatibility and mechanical properties for hard-tissue implant applications, ACS Appl. Mater. Interfaces. 7 (2015) 6351–6358. doi:10.1021/acsami.5b01193.

[6]   M. Grein, J. Gerstenberg, C. von der Heide, R. Bandorf, G. Bräuer, A. Dietzel, Niobium-containing DLC coatings on various substrates for strain gauges, Coatings. 9 (2019) 1–11. doi:10.3390/COATINGS9070417.

[7]   I. Bouabibsa, S. Lamri, F. Sanchette, Structure, Mechanical and Tribological Properties of Me-Doped Diamond-Like Carbon (DLC) (Me = Al, Ti, or Nb) Hydrogenated Amorphous Carbon Coatings, Coatings. 8 (2018) 1–15. doi:10.3390/coatings8100370.

[8]   J.C. Ding, W. Dai, T.F. Zhang, P. Zhao, J.M. Yun, K.H. Kim, Q.M. Wang, Microstructure and properties of Nb-doped diamond-like carbon films deposited by high power impulse

magnetron sputtering, Thin Solid Films. 663 (2018) 159–167. doi:10.1016/j.tsf.2018.07.012.

[9]   N. Nedfors, O. Tengstrand, E. Lewin, A. Furlan, P. Eklund, L. Hultman, U. Jansson, Structural, mechanical and electrical-contact properties of nanocrystalline-NbC/amorphous-C coatings deposited by magnetron sputtering, Surf. Coatings Technol. 206 (2011) 354–359. doi:10.1016/j.surfcoat.2011.07.021.

[10]   R. Olivares-Navarrete, J.J. Olaya, C. Ramírez, S.E. Rodil, Biocompatibility of Niobium Coatings, Coatings. 1 (2011) 72–87. doi:10.3390/coatings1010072.

[11]   S.A. Pauline, N. Rajendran, Corrosion behaviour and biocompatibility of nanoporous niobium incorporated titanium oxide coating for orthopaedic applications, Ceram. Int. 43 (2017) 1731–1739. doi:10.1016/j.ceramint.2016.08.207.

[12]   E. Asselin, T.M. Ahmed, A. Alfantazi, Corrosion of niobium in sulphuric and hydrochloric acid solutions at 75 and 95 °C, Corros. Sci. 49 (2007) 694–710. doi:10.1016/j.corsci.2006.05.028.

[13]   S.B. Lyon, Corrosion of tantalum and niobium and their alloys, Shreir's Corros. 3 (2010) 2135–2150. doi:10.1016/B978-044452787-5.00102-5.

[14]   C. Corbella, M. Vives, A. Pinyol, E. Bertran, C. Canal, M.C. Polo, J.L. Andújar, Preparation of metal (W, Mo, Nb, Ti) containing a-C:H films by reactive magnetron sputtering, Surf. Coatings Technol. 177–178 (2004) 409–414. doi:10.1016/j.surfcoat.2003.09.017.

[15]   M. Grein, R. Bandorf, K. Schiffmann, G. Bräuer, Material structure and piezoresistive properties of niobium containing diamond-like-carbon films, Surf. Coatings Technol. 357 (2019) 273–279. doi:10.1016/j.surfcoat.2018.10.008.

[16] I. Bouabibsa, S. Lamri, A. Alhussein, T. Minea, F. Sanchette, Plasma investigations and deposition of Me-DLC (Me = Al, Ti or Nb) obtained by a magnetron sputtering-RFPECVD hybrid process, Surf. Coatings Technol. 354 (2018) 351–359. doi:10.1016/j.surfcoat.2018.09.033.

[17] K. Bewilogua, C. V Cooper, C. Specht, J. Schroder, R. Wittorf, M. Grischke, Erratum to : '" Effect of target material on deposition and properties of metal-containing DLC (Me-DLC) coatings ,"' Surf. Coatings Technol. 132 (2000) 275–283. doi:10.1016/S0257-8972(00)00746-5.

[18] N. Liu, H. Zhu, Q. Wei, H. Long, Z. Deng, Z. Yu, Y. Xie, J. Wang, L. Ma, K. Zhou, A Niobium and Nitrogen Co-Doped DLC Film Electrode and Its Electrochemical Properties, J. Electrochem. Soc. 164 (2017) H1091–H1098. doi:10.1149/2.1001714jes.

[19] S. Khamseh, E. Alibakhshi, B. Ramezanzadeh, M. Ganjaee Sari, A tailored pulsed substrate bias voltage deposited (a-C: Nb) thin-film coating on GTD-450 stainless steel: Enhancing mechanical and corrosion protection characteristics, Chem. Eng. J. 404 (2021) 1–10. doi:10.1016/j.cej.2020.126490.

[20] J.C. Ding, H. Mei, S. Jeong, J. Zheng, Q.M. Wang, K.H. Kim, Effect of bias voltage on the microstructure and properties of Nb-DLC films prepared by a hybrid sputtering system, J. Alloys Compd. 861 (2021) 1–9. doi:https://doi.org/10.1016/j.jallcom.2020.158505.

[21] K. Hou, P. Yi, L. Peng, X. Lai, Niobium doped amorphous carbon film on metallic bipolar plates for PEMFCs: First principle calculation, microstructure and performance, Int. J. Hydrogen Energy. 44 (2019) 3144–3156. doi:10.1016/j.ijhydene.2018.12.040.

[22] H. Hermawan, D. Ramdan, J.R. P. Djuansjah, Metals for Biomedical Applications, in:

Biomed. Eng. - From Theory to Appl., 2011: pp. 411–430. doi:10.5772/19033.

[23] S.J. Gobbi, V.J. Gobbi, Y. Rocha, Requirements for Selection/Development of a

Biomaterial, Biomed. J. Sci. Tech. Res. 14 (2019) 1–6.

doi:10.26717.BJSTR.2019.14.002554.

[24] M. Niinomi, Metallic biomaterials, J. Artif. Organs. 11 (2008) 105–110.

doi:10.1007/s10047-008-0422-7.

[25] K. Ishihara, Highly lubricated polymer interfaces for advanced artificial hip joints through

biomimetic design, Polym. J. 47 (2015) 585–597. doi:10.1038/pj.2015.45.

[26] N. Eliaz, Corrosion of Metallic Biomaterials: A Review, Materials (Basel). 12 (2019) 1–

91. doi:10.3390/ma12030407.

[27] C.Y. Hu, T.R. Yoon, Recent updates for biomaterials used in total hip arthroplasty,

Biomater. Res. 22 (2018) 1–12. doi:10.1186/s40824-018-0144-8.

[28] M. Saini, Implant biomaterials: A comprehensive review, World J. Clin. Cases. 3 (2015)

52–57. doi:10.12998/wjcc.v3.i1.52.

[29] M.A. Hussein, A.S. Mohammed, N. Al-Aqeeli, Wear characteristics of metallic

biomaterials: A review, Materials (Basel). 8 (2015) 2749–2768. doi:10.3390/ma8052749.

[30] G. Herting, I.O. Wallinder, C. Leygraf, Metal release rate from AISI 316L stainless steel

and pure Fe , Cr and Ni into a synthetic biological medium- a comparison, J. Environ.

Monit. 10 (2008) 1092–1098. doi:10.1039/b805075a.

[31] A. Nouri, C. Wen, Introduction to surface coating and modification for metallic

biomaterials, Elsevier Ltd, 2015. doi:10.1016/B978-1-78242-303-4.00001-6.

[32] X. Jin, L. Gao, E. Liu, F. Yu, X. Shu, H. Wang, Microstructure, corrosion and tribological

and antibacterial properties of Ti–Cu coated stainless steel, J. Mech. Behav. Biomed.

Mater. 50 (2015) 23–32. doi:10.1016/j.jmbbm.2015.06.004.

[33]   ASTM International, Standard Specification for Unalloyed Titanium , for Surgical Implant Applications (UNS R50250, UNS R50400, UNS R50550, UNS R50700), 2017.

[34]   A.K. Shukla, R. Balasubramaniam, S. Bhargava, Properties of passive film formed on CP titanium , Ti–6Al–4V and Ti–13 4Al–29Nb alloys in simulated human body conditions, Intermetallics. 13 (2004) 631–637. doi:10.1016/j.intermet.2004.10.001.

[35]   K.T. Kim, M.Y. Eo, T. Thi, H. Nguyen, S.M. Kim, General review of titanium toxicity, Int. J. Implant Dent. 5 (2019) 1–12. doi:10.1186/s40729-019-0162-x.

[36]   B.D. Ratner, A.S. Hoffman, F.J. Schoen, J.E. Lemons, Biomaterials Science: An Introduction to Materials in Medicine, 2004.

[37]   D.R. Carter, W.E. Caler, D.M. Spengler, V.H. Frankel, Uniaxial fatigue of human cortical bone. The influence of tissue physical characteristics, J. Biomech. 14 (1981) 461–470. doi:10.1016/0021-9290(81)90096-8.

[38]   H.R. FELIX, R. CHOLLET, J. HARR, Use of the cell wall-less alga Dunaliella bioculata in herbicide screening tests, Ann. Appl. Biol. 113 (1988) 55–60. doi:10.1111/j.1744-7348.1988.tb03281.x.

[39]   H. Ronkainen, Tribological properties of hydrogenated and hydrogen-free diamond-like carbon coatings: Dissertation. VTT Technical Research Centre of Finland, 2001.

[40]   J. Robertson, Diamond-like amorphous carbon, Mater. Sci. Eng. R Reports. 37 (2002) 129–281. doi:10.1016/S0927-796X(02)00005-0.

[41]   S. Zhang, M. Yan, Y. Yang, Y. Zhang, F. Yan, H. Li, Excellent mechanical, tribological and anti-corrosive performance of novel Ti-DLC nanocomposite thin films prepared via magnetron sputtering method, Carbon N. Y. 151 (2019) 136–147.

doi:10.1016/j.carbon.2019.05.031.

[42] S. Zhang, W. Yue, J. Kang, Y. Wang, Z. Fu, L. Zhu, D. She, C. Wang, Ti content on the tribological properties of W/Ti-doped diamond-like carbon film lubricating with additives, Wear. 430–431 (2019) 137–144. doi:10.1016/j.wear.2019.05.002.

[43] H. Dimigen, H. Hubsch, CARBON CONTAINING LAYER, U.S. Patent 34035E, 1992.

[44] M. Eckel, G. Kampschulte, P. Markschläger, Improvements in a-C film properties by metal incorporation and intermediate layers, Surf. Coatings Technol. 74–75 (1995) 827–832. doi:10.1016/0257-8972(95)08313-8.

[45] C. Chen, W. Tang, X. Li, W. Wang, C. Xu, Structure and cutting performance of Ti-DLC films prepared by reactive magnetron sputtering, Diam. Relat. Mater. 104 (2020) 1–6. doi:10.1016/j.diamond.2020.107735.

[46] Y. Zhou, P. Guo, L. Sun, L. Liu, X. Xu, W. Li, X. Li, K.R. Lee, A. Wang, Microstructure and property evolution of diamond-like carbon films co-doped by Al and Ti with different ratios, Surf. Coatings Technol. 361 (2019) 83–90. doi:10.1016/j.surfcoat.2019.01.049.

[47] J.C. Sánchez-López, A. Fernández, Doping and Alloying Effects on DLC Coatings, in: Tribol. Diamond-Like Carbon Film. Fundam. Appl., 2008: pp. 311–328. doi:10.1007/978-0-387-49891-1_12.

[48] Y. Zhou, L. Li, W. Shao, Z. Chen, S. Wang, X. Xing, Q. Yang, Mechanical and tribological behaviors of Ti-DLC films deposited on 304 stainless steel: Exploration with Ti doping from micro to macro, Diam. Relat. Mater. 107 (2020) 1–7. doi:10.1016/j.diamond.2020.107870.

[49] W. Dai, P. Ke, M.W. Moon, K.R. Lee, A. Wang, Investigation of the microstructure, mechanical properties and tribological behaviors of Ti-containing diamond-like carbon

films fabricated by a hybrid ion beam method, Thin Solid Films. 520 (2012) 6057–6063. doi:10.1016/j.tsf.2012.04.016.

[50]   H.W. Choi, J.H. Choi, K.R. Lee, J.P. Ahn, K.H. Oh, Structure and mechanical properties of Ag-incorporated DLC films prepared by a hybrid ion beam deposition system, Thin Solid Films. 516 (2007) 248–251. doi:10.1016/j.tsf.2007.06.154.

[51]   W. Dai, A. Wang, Synthesis, characterization and properties of the DLC films with low Cr concentration doping by a hybrid linear ion beam system, Surf. Coatings Technol. 205 (2011) 2882–2886. doi:10.1016/j.surfcoat.2010.10.057.

[52]   J. Cui, L. Qiang, B. Zhang, X. Ling, T. Yang, J. Zhang, Mechanical and tribological properties of Ti-DLC films with different Ti content by magnetron sputtering technique, Appl. Surf. Sci. 258 (2012) 5025–5030. doi:10.1016/j.apsusc.2012.01.072.

[53]   M. Zhang, T. Xie, X. Qian, Y. Zhu, X. Liu, Mechanical properties and biocompatibility of Ti-doped diamond-like carbon films, ACS Omega. 5 (2020) 22772–22777. doi:10.1021/acsomega.0c01715.

[54]   C.A. Love, R.B. Cook, T.J. Harvey, P.A. Dearnley, R.J.K. Wood, Diamond like carbon coatings for potential application in biological implants - A review, Tribol. Int. 63 (2013) 141–150. doi:10.1016/j.triboint.2012.09.006.

[55]   N. Vidakis, A. Antoniadis, N. Bilalis, The VDI 3198 indentation test evaluation of a reliable qualitative control for layered compounds, J. Mater. Process. Technol. 143–144 (2003) 481–485. doi:10.1016/S0924-0136(03)00300-5.

[56]   S. Affatato, M. Frigo, A. Toni, An in vitro investigation of diamond-like carbon as a femoral head coating, J. Biomed. Mater. Res. 53 (2000) 221–226. doi:10.1002/(SICI)1097-4636(2000)53:3<221::AID-JBM6>3.0.CO;2-Z.

[57]   V. Saikko, T. Ahlroos, O. Calonius, J. KeraKnen, Wear simulation of total hip prostheses with polyethylene againstCoCr, alumina and diamond-like carbon, Biomaterials. 22 (2001) 1507–1514. doi:10.1016/s0142-9612(00)00306-9.

[58]   H. Frey, H.R. Khan, Handbook of Thin-Film Technology, 2015.

[59]   ASTM F1537, Standard Specification for Wrought Cobalt-28Chromium-6Molybdenum Alloys for Surgical Implants, ASTM Int. (2011) 1–4. doi:10.1520/F1537-20.2.

[60]   I.V. Tudose, F. Comanescu, P. Pascariu, S. Bucur, L. Rusen, F. Iacomi, E. Koudoumas, M.P. Suchea, Chemical and physical methods for multifunctional nanostructured interface fabrication, Elsevier Inc., 2019. doi:10.1016/B978-0-12-814401-5.00002-5.

[61]   I. Childres, L.A. Jauregui, W. Park, H. Caoa, Y.P. Chena, Raman spectroscopy of graphene and related materials, New Dev. Phot. Mater. Res. (2013) 403–418.

[62]   D. Ugur, I. Efeoglu, S. Altintas, Characterization of Titanium and Niobium Doped DLC Films Grown By Pulsed dc PVD - Closed Field Unbalanced Magnetron Sputtering (CFUBMS) Method, in: Int. Jt. Tribol. Conf., 2019: pp. 1–3.

[63]   H. Niakan, Q. Yang, J.A. Szpunar, Structure and properties of diamond-like carbon thin films synthesized by biased target ion beam deposition, Surf. Coatings Technol. 223 (2013) 11–16. doi:10.1016/j.surfcoat.2013.02.019.

[64]   A. Darlinski, J. Halbritter, Angle resolved XPS studies of oxides at Nb- NbN-, NbC- and Nb3Sn- surfaces, SURFAC'E INTERFACE Anal. 10 (1987) 223–237. doi:10.1109/TMAG.1987.1065079.

[65]   M. Grundner, J. Halbritter, XPS and AES studies on oxide growth and oxide coatings on niobium, J. Appl. Phys. 51 (1980) 397–405. doi:10.1063/1.327386.

[66]   L. Qiang, B. Zhang, Y. Zhou, J. Zhang, Improving the internal stress and wear resistance

of DLC film by low content Ti doping, Solid State Sci. 20 (2013) 17–22. doi:10.1016/j.solidstatesciences.2013.03.003.

[67]   N.W. Khun, E. Liu, Corrosion Behavior of Aluminum Doped Diamond-Like Carbon Thin Films in NaCl Aqueous Solution, J. Nanosci. Nanotechnol. 10 (2010) 4767–4772. doi:10.1166/jnn.2010.1682.

[68]   L. Qiang, K. Gao, L. Zhang, J. Wang, B. Zhang, J. Zhang, Further improving the mechanical and tribological properties of low content Ti-doped DLC film by W incorporating, Appl. Surf. Sci. 353 (2015) 522–529. doi:10.1016/j.apsusc.2015.06.040.

[69]   C. Wei, C. Chen, The effect of thermal and plastic mismatch on stress distribution in diamond like carbon fi lm under different interlayer / substrate system, Diam. Relat. Mater. 17 (2008) 1534–1540. doi:10.1016/j.diamond.2008.03.004.

[70]   American Elements. Cobalt Chromium Molybdenum Alloy, (n.d.). https://www.americanelements.com/cobalt-chromium-molybdenum-alloy-105525-46-0#section-properties (accessed March 24, 2021).

[71]   Goodfellow. Niobium (Nb) Material Information, (n.d.). http://www.goodfellow.com/A/Niobium.html (accessed March 24, 2021).

[72]   D. Caschera, F. Federici, L. Pandolfi, S. Kaciulis, M. Sebastiani, E. Bemporad, G. Padeletti, Effect of composition on mechanical behaviour of diamond-like carbon coatings modified with titanium, Thin Solid Films. 519 (2011) 3061–3067. doi:10.1016/j.tsf.2010.12.031.

[73]   J. Pu, G. Zhang, S. Wan, R. Zhang, Synthesis and characterization of low-friction Al-DLC films with high hardness and low stress, J. Compos. Mater. 49 (2015) 199–207. doi:10.1177/0021998313515291.

[74] W. Dai, G. Wu, A. Wang, Preparation, characterization and properties of Cr-incorporated DLC films on magnesium alloy, Diam. Relat. Mater. 19 (2010) 1307–1315. doi:10.1016/j.diamond.2010.06.018.

[75] W. Shao, Y. Zhou, Z. Shi, L. Rao, T. Hu, X. Xing, Q. Yang, Effects of carbide forming elements Me on residual stress and mechanical properties of DLC films by molecular dynamics simulation, Mater. Today Commun. 23 (2020) 1–9. doi:10.1016/j.mtcomm.2020.100946.

[76] N. Cansever, Properties of niobium nitride coatings deposited by cathodic arc physical vapor deposition, Thin Solid Films. 515 (2007) 3670–3674. doi:10.1016/j.tsf.2006.10.133.

[77] R.D. Boehm, C. Jin, R.J. Narayan, Carbon and Diamond, Compr. Biomater. II. 1 (2017) 145–164. doi:10.1016/B978-0-08-100691-7.00216-0.

[78] M. Braic, V. Braic, M. Balaceanu, A. Vladescu, C.N. Zoita, I. Titorencu, V. Jinga, F. Miculescu, Preparation and characterization of biocompatible Nb-C coatings, Thin Solid Films. 519 (2011) 4064–4068. doi:10.1016/j.tsf.2011.01.193.

[79] L.P. Ward, P.K. Datta, Physical Properties of Nb Coatings for Biomedical Applications, Key Eng. Mater. 72–74 (2009) 505–522. doi:10.4028/www.scientific.net/kem.72-74.505.